Multistage Fluid Evolution and P-T Path at Ity Gold Deposit and Dahapleu Prospect (Western Ivory Coast)

Yacouba Coulibaly, Michel Cathelineau, Marie-Christine Boiron

minerals

MDPI

Article

Multistage Fluid Evolution and P-T Path at Ity Gold Deposit and Dahapleu Prospect (Western Ivory Coast)

Yacouba Coulibaly [1], Michel Cathelineau [2,*] and Marie-Christine Boiron [2]

[1] LGRME, UFR Sciences de la Terre et des Ressources Minières, Université Félix Houphouet-Boigny d'Abidjan Cocody, BP 582, Abidjan 22, Côte d'Ivoire; coulibaly.yacouba3@ufhb.edu.ci
[2] Université de Lorraine, CNRS, GeoRessources, 54000 Nancy, France; marie-christine.boiron@univ-lorraine.fr
* Correspondence: michel.cathelineau@univ-lorraine.fr

Abstract

Gold mineralisation at Ity (Ivory Coast) is spatially associated with skarns formed at contacts between carbonate-rich Birimian volcano-sedimentary rocks and felsic intrusions, whereas at Dahapleu, a nearby skarn-free prospect, gold occurs in structurally controlled shear zones. Gold occurs as native gold in pyrite or as a Bi–Te–Au–Ag telluride assemblage. Fluid inclusion data indicate that Ity formed through a hybrid model: a mesothermal orogenic gold system dominated by CO_2–CH_4 fluids at >350 °C, superimposed on earlier skarn mineralisation characterised by saline fluids. At Dahapleu, no skarn fluids were identified, but volatile-rich inclusions with more variable signatures (CO_2, CO_2–CH_4, CO_2–N_2) indicate metamorphic fluids circulating in convective, fault-related systems and recording distinct fluid–rock interactions. The Ity–Dahapleu mineralising system thus displays fluid inclusion characteristics typical of mesothermal orogenic gold systems, likely at higher temperatures than most West African Birimian deposits. Overall, the Ity system reflects a long-lived thermal anomaly driving fluid circulation and metal deposition, with successive favourable events: rapid exhumation of hot lithospheric crust, granite intrusion, and skarn formation, followed by shear deformation and hydrothermal activity.

Keywords: orogenic gold deposits; fluid inclusions; P-T conditions; Skarn; Birimian; Ity (Ivory Coast)

Academic Editors: Panagiotis Voudouris, Vasilios Melfos, Grigorios Aarne Sakellaris and Ferenc Molnár

Received: 18 July 2025
Revised: 23 August 2025
Accepted: 25 August 2025
Published: 28 August 2025

Citation: Coulibaly, Y.; Cathelineau, M.; Boiron, M.-C. Multistage Fluid Evolution and P-T Path at Ity Gold Deposit and Dahapleu Prospect (Western Ivory Coast). *Minerals* **2025**, *15*, 918. https://doi.org/10.3390/min15090918

1. Introduction

Paleoproterozoic Birimian terranes of the West African Craton host numerous world-class gold deposits, many of which are structurally controlled and formed in orogenic or intrusion-related settings ([1–3], and references herein). These gold systems, which account for a significant share of Africa's gold production, remain the focus of intense exploration due to their structural complexity [4–6], metallogenic diversity, and potential for supergene enrichment. Understanding the geological processes that control mineralisation—including the timing and nature of magmatic activity, the role of deformation, and the superimposed weathering profiles—is therefore critical for both scientific and economic purposes [3,7–10].

The Ity gold district, located in western Ivory Coast within the Man-Leo Shield, provides a compelling case study of such a hybrid system. It combines features of skarn-type and shear-hosted mineralisation, spatially associated with Paleoproterozoic volcanic and volcano-sedimentary units intruded by granodioritic to dioritic plutons. The deposit has been affected by multiple Eburnean deformation phases (~2.1–2.0 Ga), leading to the

development of ductile shear zones and brittle fault structures that host significant gold-bearing quartz-carbonate vein networks [11]. Gold at Ity occurs in two principal settings: (1) skarns formed at the contact between carbonate-rich metasediments and felsic intrusives marked by Fe-rich alteration (ankerite, pyrite, chalcopyrite); (2) structurally controlled quartz veins localised within regional-scale shear zones. These two styles are often spatially and temporally associated, suggesting a continuum of hydrothermal processes linked to magmatic intrusion and tectonic activity. Overprinting this primary mineralisation is an extensive tropical weathering profile that has led to significant supergene enrichment, particularly within lateritic and saprolitic horizons [12–15]. This primary gold enrichment deposit, however, is poorly understood in detail, as most early studies focused on the outcropping supergene mineralisation. The primary mineralisation was initially associated with a magnetite-skarn type [16]. More recently, Milési et al. [7,8] suggested that the presence of residual blocks of ore-bearing quartz and/or variably oxidised sulphides in the weathered rocks might indicate that the primary mineralisation could belong to a mesothermal gold quartz vein with either auriferous arsenopyrite or rare polymetallic sulphide hosted by various lithologies (metasedimentary, metavolcanic, or granitoids).

Up to now, no data were available on the ore-forming fluids and processes for the formation of this deposit, as most of the available material was deeply affected by the laterite profile. Thus, this study contributes to the understanding of the genesis of primary ores that form the Ity deposit and the Dahapleu gold prospect, located near the Ity mine, on the other side of the Cavally River, within a lengthened anomalous SW-NE zone.

This study aims to clarify the geological and metallogenic framework of the Ity gold system, with a focus on the interplay between fluid pathways, metal deposition, and water–rock interactions. The objective of this work is to describe the primary mineralisation, especially the paragenetic assemblage related to primary ore, and the succession of fluid circulation events by studying the relationships between ore minerals and paleofluid features. Special attention has been paid to identifying the fluid sequence and determining the paleofluid chemistry using microthermometry and Raman spectroscopy. Finally, the P-T-t path for the history of the primary ore deposit has been reconstructed. The results are discussed and compared with those of previous studies from Birimian terranes in neighbouring countries to establish a genetic model.

2. Geological Setting

2.1. Regional Geology

The southern part of the West African craton, known as the Man Shield, was stabilised at approximately 1.6 billion years ago [17]. This cratonic domain, separated into two domains by the major sub-meridian Sassandra strike-slip fault [18], consists of an Archean core (3.4 to 2.6 Ga) and Lower Proterozoic (2.2 to 1.9 Ga) terranes [7,18,19]. The Archean domain, located on the West side of the Sassandra fault and traditionally called "Kenema–Man domain", is composed of rocks that were affected by two major orogenic events: the Leonian (3.5 to 2.9 Ga) and the Liberian (2.9 to 2.6 Ga) cycles [17,18,20–23]. The second domain, the so-called "Baoulé–Mossi domain", is located on the eastern side of the Sassandra fault and contains Lower Proterozoic terranes and relics of the Archean formations that were deformed during Eburnean orogeny (2.4 to 1.6 Ga, [17]). The Lower Proterozoic terranes, the so-called Birimian formations, were deformed (folded and schistosed) during the Eburnean orogeny (2.5 to 2.1 Ga). The Birimian units formed as a part of a significant episode of the crust-forming event between 2.25 and 2.05 Ga [10,24–26] and are accompanied by the intrusion of several suites of granitoids [27].

2.2. The Ity Deposit

The Ity deposit (N 7°01′8.7″ and W 5°31′18.1″) is located near the village of Ity, 30 km South of Man, in the western part of the Ivory Coast, close to the Liberian border.

Ity is the oldest gold mine in the Ivory Coast, with work starting in 1950 and regular production since 1991, when the first gold was poured by Société des Mines d'Ity (SMI). At the time, the mine produced more than half of the Ivory Coast's gold. From 2012, the company was owned by the La Mancha group and the Société d'État pour le développement minier de Côte d'Ivoire (SODEMI: Société pour le Développement Minier de la Côte d'Ivoire). Endeavour acquired the Ity mine in 2015 and subsequently increased its stake to 85% in 2018, following the construction of a new ore processing plant. This stake was supplemented by the Ivorian state (10%) and the state-owned SODEMI (5%).

The mine has produced more than 1.4 million ounces of gold since 1991, 343 koz in 2024, and is expected to deliver between 290 and 330 koz in 2025. Proven and probable reserves are estimated at 11 million metric tons of ore at 0.91 ppm and 67 million metric tons at 1.4 ppm, respectively, totalling around 3000 koz (Endeavour data, https://www.endeavourmining.com/our-portfolio/reserves-and-resources, accessed on 15 June 2025). The ore type is considered particular because the main exploited gold ore is located in the weathered parts of the deposit [7,8,12], which are developed on marble and ortho-amphibolite rocks.

2.3. The Geology of the Toulepleu–Ity Klippe

The studied area is located in the Kenema–Man domain of the West African craton but belongs to the Toulepleu–Ity volcano-clastic unit of Birimian age [28,29]. This unit, approximately 8 to 30 km in width, lies in tectonic contact over Archean supracrustal rocks (<2.68 Ga; [19] (Figure 1). The unit displays an NNE-SSE trending, up to 100 km in length, in the Ivorian territory and is extended into Liberia [30].

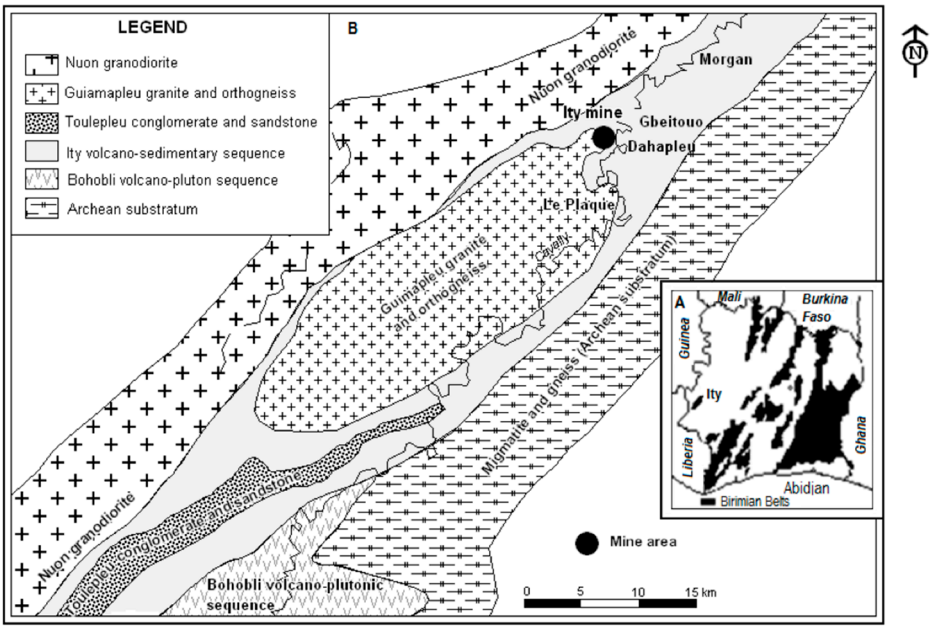

Figure 1. (**A**) Map of the Ivory Coast with location of the Birimian belt. (**B**) Geological map of the Toulepleu–Ity klippe with location of the studied zones (modified from [31]).

The Toulepleu–Ity unit, defined as the «Toulepleu–Ity klippe» [28], is interpreted as a strip of Lower Proterozoic (Birimian) rocks, thrusted during the collisional phase of the Eburnean orogenesis (D1) and preserved in its center from a later D2 deformation stage affecting the Kenema–Man terranes. In fact, during the Eburnean orogeny [18,32,33], the

rocks were affected by a D1 tangential deformation event, followed by a D2 transcurrent tectonic stage at approximately 2.1 Ga [28].

This klippe shows the following litho-structural succession over the Archean basement [28]. The oldest and central Birimian units in the mine area belong to the Ity sequence, which consists of banded mafic amphibolites (metabasalts) overlain by fine-grained sediments with intercalated limestones (200 to 300 m in width), jasperoids, black schists, and more acidic volcano-clastic rocks. This sequence is affected by the two Eburnean deformation stages (D1 and D2). The Toulepleu series, made of conglomerates and sandstones, is observed unconformably over the Ity sequence.

Felsic sub-volcanic rocks (gabbros, hypovolcanic quartz diorites, and granites) intruded the Ity sequence, probably at the onset of D2 deformation. These intrusive rocks have produced contact metamorphism, particularly the formation of skarns in carbonated rocks. These skarns and marbles occur near the contact with the intrusive bodies. The D2 phase is synchronous with metamorphism of an intensity characteristic of the epizonal/mesozonal boundary [28]. At the syn-D2 stage, the Mg-hornblende-plagioclase-calcite and green hornblende-chlorite-epidote parageneses recorded a retrograde metamorphic evolution from 600 °C and 400 MPa to 580 °C and 280 MPa [34]. In the Ity deposit, contact metamorphism is provoked by the intrusion of the Mount Zia granite [16]. For these authors, mineralisation occurred at very high temperatures, ranging from approximately 500 to 600 °C.

The Toulepleu–Ity unit is bounded (i) to the SE by the Archean basement, known as the "gneissic basement" in the mine area and containing migmatite, gneiss, and banded iron formations (BIF) and (ii) to the NW by an abnormal contact with the "anatexic" granodiorite of Nuon, including gneiss and migmatites.

3. Materials and Methods

Representative samples of fresh facies from the mineralised area were collected from the Flotouo pit (Ity Mine) (Table 1), including marbles, skarns, and massive sulphides. Core samples were also taken from the Dahapleu prospect, located close to the Ity mine (Table 1).

Table 1. Characteristics of the selected samples from the Ity deposit and Dahapleu prospect.

Sample	X utm 29	Yutm 29	Z (m)	Depth (m)	Lithology	Mineralogy	Mineralization	Au (g/t)
ITY (Flotouo pit)								
FLO W03	598181	759945	215		Marble	**cal**-px-am-phl	py-po-cpy-cob	2
FLO W04	598181	759945	216		Marble	**cal**-am	psil-vat	~2
FLO E03	598260	760035	235		Marble	**cal**-px-am-phl-ms-or.	gn-psil	~2
FLO E04	598260	760035	235		Marble	**cal**-am	cpy	~2
FLO E05	598267	760021	235		Marble	cal	py-psil	~2
FLO E06	598270	760023	235		Marble	**cal**-am-px-phl	py-po-psil	~2
FLO E08	598260	760059	240		Massif sulfides		qz-**py**-po-cpy-Te (Ag-Au)-**py**	6
FLO E09	598255	760056	240		Skarn	grt	mt-po-cpy-**py**	n.d.
FLO E10	598244	760044	240		Magnetite Skarn		**mt**-po-cpy-py-sph	n.d.
Dahapleu prospect								
SD 159-1	600295	758464	193	78.00	Sch.quartzite	**qz**-ms-(mc-or-pl)	py-cpy-sph-asp-boul-gn-po-en-td-Ag-Au	1.98
SD 159-2	600288	758470	204	50.50	Sch.quartzite	**qz**-ms-(mc-or-pl-cal-tur)	py-cpy-asp-po	1.2
SD 160-1	600258	758501	195	71.20	Sch.quartzite	**qz**-ms-(or-cal)	py	2.94
SD 164-1	600539	758417	234	25.60	Sch.quartzite	**qz**-ms-(or)	py	9.92
SD 164-2	600539	758417	233	26.60	Sch.quartzite	**qz**-ms-(tur)	py	1.84
SD 172-1	600481	758408	235	23.60	Sch.quartzite	**qz**-ms-(or)	py	1.31

cal: calcite; px: pyroxene; am: amphibole; phl: phlogopite; mc: microcline; or: orthoclase; grt: garnet; qz: quartz; ms: muscovite; pl: plagioclase; tur: toumaline; py: pyrite; po: pyrrhotite; cpy: chalcopyrite; cob: cobaltite; psil: psilomelane; vat: vaterite; gn: galena; Te: tellurides; Ag: silver; Au: gold; mt: magnetite; sph: sphalerite; asp: arsenopyrite; boul: boulangerite; ten: tennantite; td: tetrahedrite. n.d: not determined.Sch: schsitosed. The mining company estimates the gold content to be around two parts per million for the sampled area.

3.1. Mineralogy and Petrography

The study is based on macroscopic observations and sampling made during fieldwork, as well as petrographic observations of thin polished sections using optical and scanning electron microscopy (SEM). SEM microphotographs were obtained using a HITACHI S2500 instrument equipped with a KEVEX (delta system) energy dispersive detector (Hitachi High-Tech Co, Harumi, Japan) at Nancy Université (Nancy, France). Electron microprobe analyses were conducted on a Cameca SX 100 electron microprobe (CAMECA SAS, Gennevilliers, France) at Nancy Université (Nancy, France) using the following analytical conditions: 10 kV, 6 nA, a diameter of 1 micrometre for the investigated area, a correction program (ZAF Cor2), and a maximum analytical error of 3% of the total.

3.2. Microthermometry and Raman Spectroscopy

Fluid inclusion microthermometry was carried out at UMR G2R, now GeoRessources, Université de Lorraine, France. Microthermometric characterisation of the fluids was performed on wafers using a Chaix–Meca heating–freezing stage [35] and a Linkham TMS 94 stage. Molar fractions of CO_2, CH_4, N_2, and H_2S were determined in individual fluid inclusions using a DILOR-LABRAM Raman spectrometer (Jobin Yvon, Longjumeau, France) at GeoRessources, Nancy. Molar fractions of NaCl, molar volume, bulk composition, and P-T parameters were determined by considering results from microthermometry and Raman analysis. Bulk composition and molar volume were computed from the P-V-T-X properties of individual inclusions in the C-O-H-S system [36–39]. The P-T properties were modelled using the V-X data and the equation of state from [40], revised by [41] for volatile-rich fluid inclusions. For aqueous fluids, data from [42] for the H_2O-NaCl system were used.

The notation for fluid inclusion types follows the nomenclature previously published [43], which considers the nature of the dominant chemical phases and the associated phase changes. It is based on the total homogenisation Th (L-V to the vapour noted V, L-V to the liquid noted L) and the quantity of C-H-O-(N-S) species detectable by Raman spectroscopy (subscript c, when C-H-O-N-S species are the only components and water is not visible, and w when C-H-O-(N-S) species are not detected by any method).

4. Results

4.1. Petrography

Petrographic examination of the samples listed in Table 1 complements previous descriptions conducted by the mining company [44]. A synthetic overview is provided in the following paragraphs. The enclosing rocks of the Ity deposit are exclusively composed of igneous, mostly basic rocks, and sedimentary carbonate-rich rocks, mostly marbles and skarns (Figure 2A–D and Figure 3A–E) and quartzites (Figure 2E,F; Figure 3F–H). From top to bottom, the sequence is composed of 75 m of marbles, calco-magnesian hornfels, and skarns, overlain by more than 50 m of ortho-amphibolites. Thin intercalations of ortho-leptynites occur within this sequence.

4.1.1. Basic Series

Amphibolites are generally free of quartz and exhibit the relict texture of volcanic or sub-volcanic rocks. These rocks are mainly composed of plagioclase, epidote, hornblende, biotite, and chlorite. The inherited paragenesis is composed of clinopyroxene (uralite cores in amphiboles) and plagioclase (andesine). The amphibolite facies metamorphism is characterised by the presence of magnesiohornblende, biotite, oligoclase (plagioclase), calcite, and quartz. Plagioclase composition varies from An25-30 to An60. Accessory minerals are ilmenite, apatite, and allanite. Green hornblende, epidote, calcite, titanite

and chlorite were formed during later retrograde stages. At the base of the amphibolite sequence, quartz is more abundant.

The dioritic or gabbroic facies are grey to black, with a grey-blue hue, and display a micro-granular texture (Figure 3A). The primary minerals are plagioclase, clinopyroxenes of augite-aegyrine type, green hornblendes, biotites, and a relatively small amount of quartz. Plagioclase compositions vary from albite to labradorite. Accessory minerals are zircon, sphene, late calcite, and florencite-bearing apatites. Amphibole, clinopyroxene, and biotite minerals show a moderate alteration to epidote and chlorite. A particular facies of this rock exhibits 25% garnet (andradite type), sodic plagioclases, and acicular tremolite.

Chlorite and garnet metatuffs exhibit two facies: (i) a green hyaline part showing several geodes filled with lamellar zeolites and globular concretions of chalcedony, and (ii) a green deformed and laminated part showing ferromagnesian chlorites and garnet (andradite). Apatite and florencite are observed.

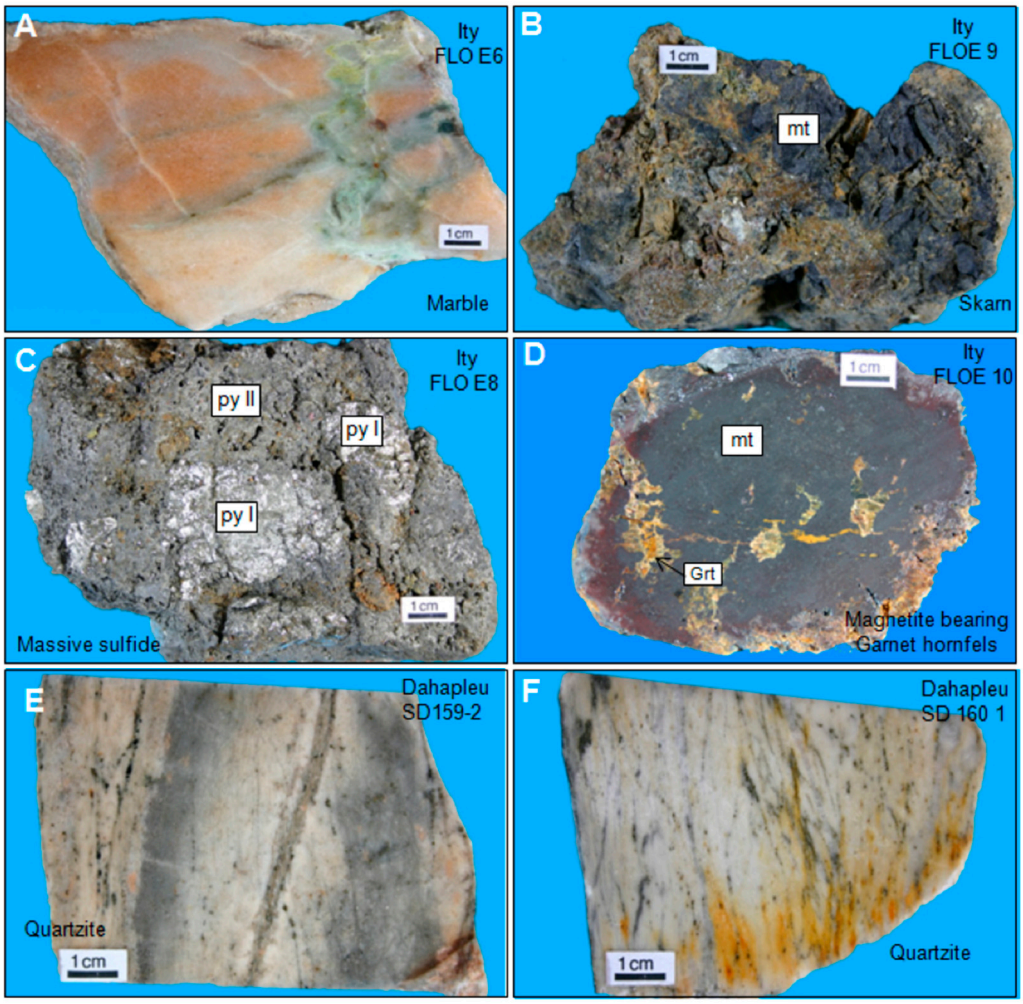

Figure 2. Representative samples from the Ity deposit and Dahapleu prospect. (**A**) Marbles with silicate mineral planes (green). (**B**) Magnetite (mt) bearing skarn. (**C**) Massive sulphide showing the two types of pyrite (py I: pyrite I, py II: pyrite II). (**D**) Magnetite-bearing garnet (Grt) hornfeld. (**E**,**F**) Quartzite containing numerous sulphide inclusions.

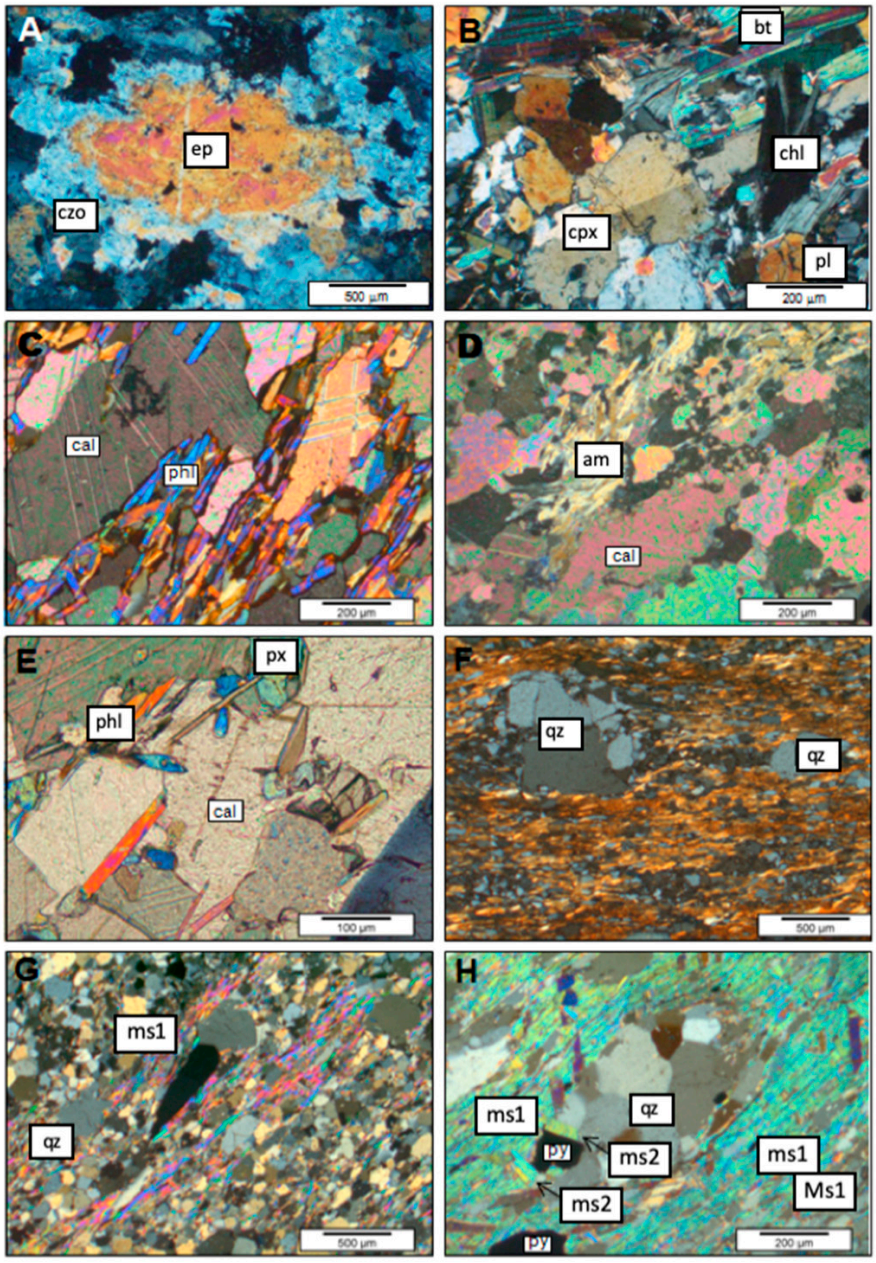

Figure 3. Petrographic characteristics of the Ity and Dahapleu rocks. (**A**) Epidotite showing two generations of epidote: clinozoïsite (czo) and other epidote type (ep). (**B**) Microdiorite showing clinopyroxene (cpx)-biotite (bt)-plagioclase (pl)-chlorite (chl) association. (**C**) Skarn showing calcite (cal) and phlogopite (phl) association. (**D**) Amphibole (amp) bearing skarn. (**E**) phlogopite and pyroxene (px) bearing skarn. (**F**) Quartzite showing quartz deformation. (**G**) Quartzite showing quartz (Qz)- muscovite 1 (Ms1)- sulphide association. (**H**) Quartzite showing quartz-muscovite 1(ms1)- muscovite 2 (ms2)-pyrite (py) association. Optical and scanning electron microscopy, complemented by electronic microprobe analysis of the mineralised samples, reveal that a magnetite-pyrite assemblage predominates in the Ity sulphide ore.

4.1.2. Felsic Series

Two types were observed as thin intercalations within amphibolites: (i) ortho-leptynite, where old plagioclase (An10-15) phenocrysts are distinguished within a quartz-albite mesostasis; (ii) a second rock type is characterised by intergrown plagioclases, interstitial quartz, large amphibole crystals, and small amounts of epidote, biotite, and chlorite.

4.1.3. Marbles, Skarns, and Hornfels

Marbles are observed at the top of the unaltered sequence. It constitutes the footwall of the weathering mineralisation. The marbles display a granoblastic texture and are mainly composed of calcite, accounting for more than 80%–90% of the volume. However, variable amounts of silicate minerals (amphibole, pyroxene, phlogopite, rare microcline, and orthoclase) and sulphide minerals are observed (Figure 2A–D, Table 1). Silicate minerals are locally concentrated in planar layers. Phlogopite is often oriented. Amphibole is frequently altered into chlorite. The composition of unaltered amphibole exhibits three types: magnesiohornblende, actinolite, and tremolite. Pyroxene crystals show a composition varying between pure diopside and salite.

The Ca-Mg-rich hornfels are fine-grained and always contain small amounts of carbonates and variable amounts of quartz. Several mineralogical associations were observed: (i) diopside, epidote (alteration), garnet; (ii) pyroxene and amphibole; (iii) amphibole.

The skarns are observed inside the marble series. Several types of skarns can be distinguished as a function of the predominant mineral phase: (i) clinopyroxene; (ii) clinochlore; (iii) vesuvianite; (iv) garnet. The latest skarn type (Figure 2B) is mainly composed of garnet (andradite) and contains mineralisation made of magnetite and sulphides (pyrite, pyrrhotite, chalcopyrite). Skarns are crosscut by rare veinlets of microcline and/or anhydrite [16]. The marbles and skarns contain approximately 2 ppm gold, as estimated by the mining company. The list of studied samples is provided in Table 1. Lajoinie and Fonteilles [16] consider that Cu-Mo(W) anomalies are related to the skarn stage.

The so-called "Epidote-rich skarns" defined by [44] are the greenstone series that show granoblastic texture varying between equigranular and heterogranular. They contain feldspaths (mainly plagioclase and rare microcline) and amphibole or pyroxene, which are highly altered into epidote. Accessory minerals are sphene with anatase inclusions, apatite, and zircon. Secondary minerals are epidote, anatase, serpentine, calcite, iron oxides, and hydroxides (rich in Mn and Ba). Epidote chemically close to clinozoïsite is abundant (20 to 85% of the rock) and accompanied by vesuvianite (Figure 3A). Both minerals are observed within the matrix or as veinlet infillings, sometimes associated with quartz. Quartz is the late infillings of veinlets and geodes.

4.1.4. Metamorphic Units from the Dahapleu Prospect

The quartzites are not homogeneous. They are mainly composed of white fine zones (containing quartz, muscovite, and K-feldspars), which alternate with fine-grained dark zones containing sulphide minerals (Figure 2E,F). These rocks have a schistose structure and a microgranoblastic to lepidoblastic texture, containing recrystallised quartz, white mica (muscovite), and sometimes rare crystals of tourmaline and feldspars (microcline and plagioclase) (Figure 3F–H). It contains sulphides within the schistosity planes and some rare tourmaline crystals. Quartz-filled fractures are locally observed.

5. Ore Assemblage

5.1. Ity Deposit

Figures 4 and 5 provide a paragenetic sequence and related representative microphotographs of the ores

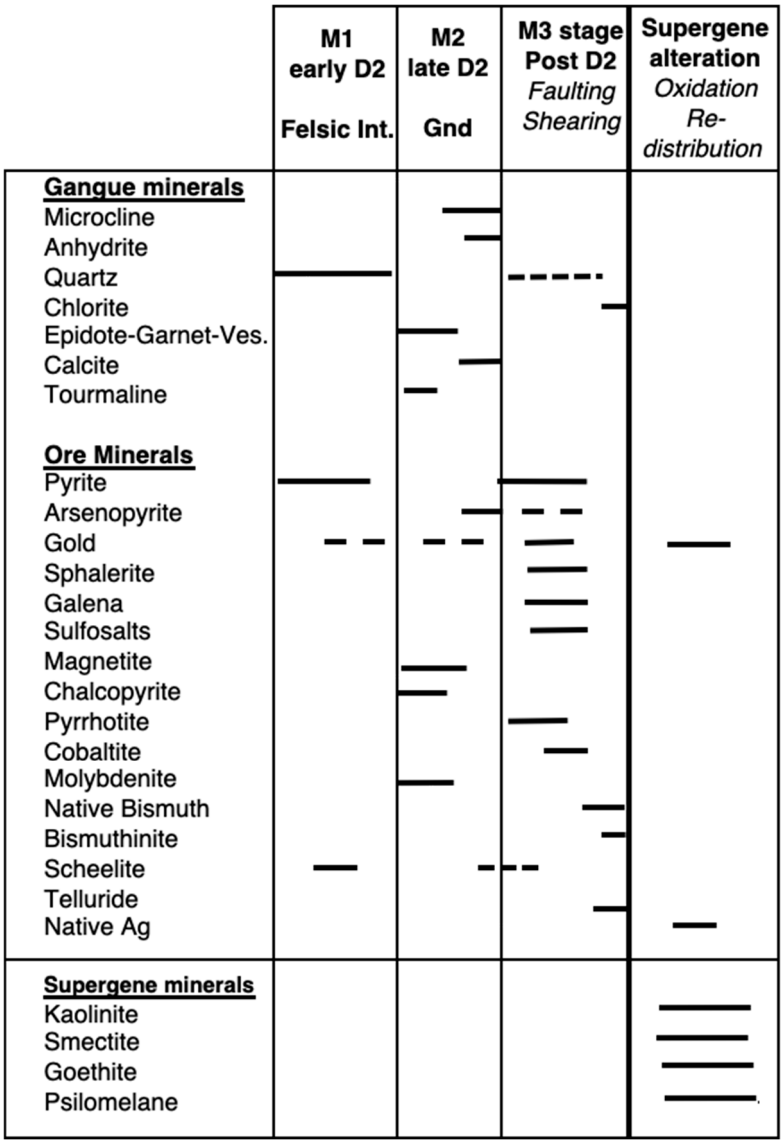

Figure 4. Paragenetic sequence of the main minerals observed in the Ity gold deposit. Ves: vesuvianite; felsic int: felsic intrusive dykes; gnd: granodiorite.

5.1.1. Enclosing Rocks

The enclosing rocks of the Ity gold mine show a weak, dispersed mineralisation, which appears either as disseminated or as fissural. Marbles show gold content close to 2 g/t. Disseminated ores are observed in all types of enclosed rocks and are composed of pyrite, chalcopyrite, pyrrhotite, cobaltite (Figure 5A), and galena.

Two generations of veins are distinguished: (i) syn-metamorphic veinlets showing the following succession of mineral associations: (a) quartz–chlorite–epidote; (b) microcline, quartz, calcite, pyrite; (c) tourmaline, quartz, chlorite, pyrite; (ii) post-metamorphic veinlets with two mineral associations: calcite–chlorite–hematite and pyrite–chalcopyrite. A series of successive infillings is observed in veinlets: (i) molybdenite, magnetite; (ii) molybdenite, pyrite; (iii) pyrite, chalcopyrite; (iv) pyrite, scheelite. The gangue is primarily composed of quartz, often associated with chlorite, epidote, microcline, anhydrite, tourmaline, or calcite.

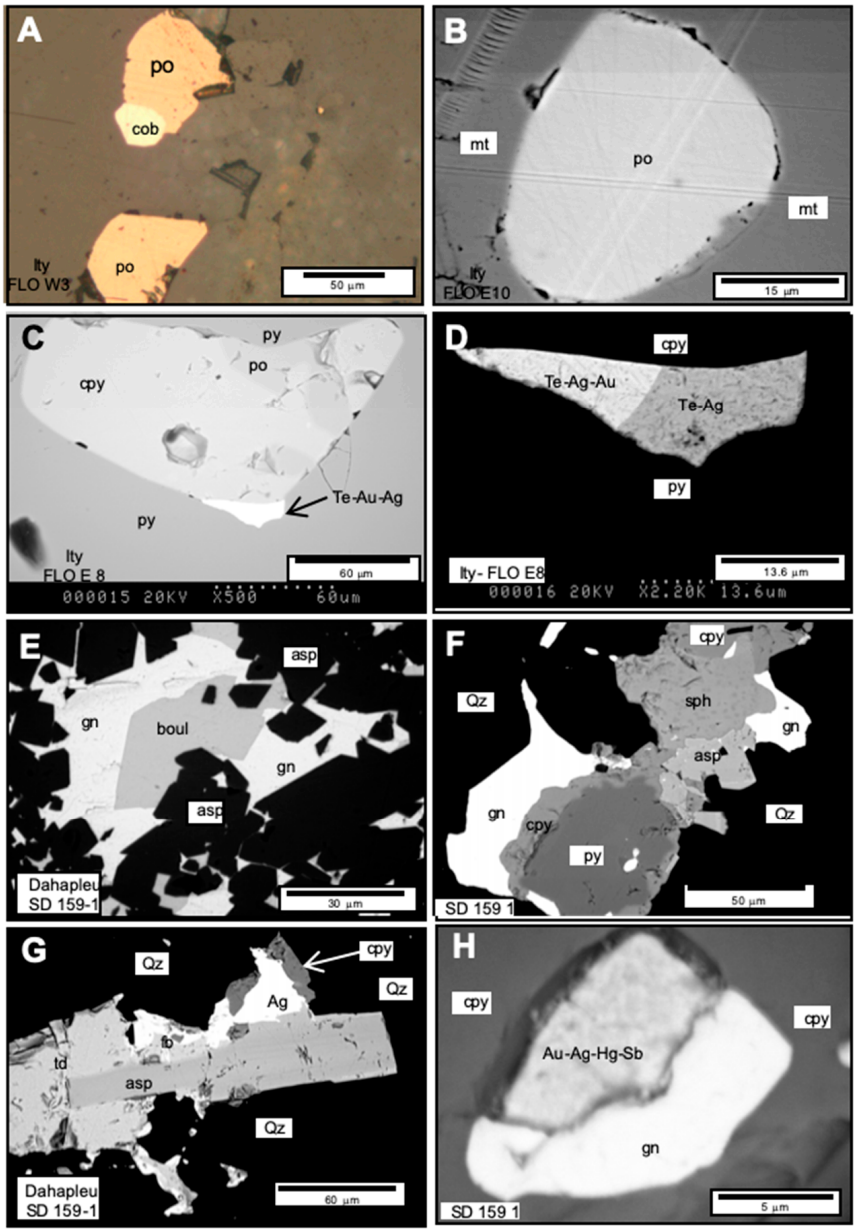

Figure 5. Photomicrographs of the mineral associations. Ity deposit: (**A**) Pyrrhotite (po)-cobaltite (cob) association. (**B**) Pyrrhotite inclusion in magnetite (mt). (**C**) Chalcopyrite (cpy), pyrrhotite, and Au-Ag telluride inclusions in pyrite (py). (**D**) Detail of the Au-Ag telluride inclusions. Dahapleu prospect: (**E**) Arsenopyrite (asp)-galena (gn)-boulangerite (boul). (**F**) Pyrite-chalcopyrite-sphalerite-galena-arsenopyrite. (**G**) Tetrahedrite (td)-freibergite (fb)- arsenopyrite–chalcopyrite–native silver. (**H**) Galena and Au-Ag-Hg-Sb mineral inclusions in chalcopyrite.

Enclosing rocks (basic formations in particular) are characterised by a greenschist facies assemblage: quartz, K-feldspar, epidote-calcite (±tourmaline, anhydrite). The same minerals are found as syn-metamorphic veinlets. The post-metamorphic veinlets are filled either by calcite, chlorite, hematite, or pyrite–chalcopyrite.

5.1.2. Mineralised Samples

Because the Ity mineralisations are only exploited in the surficial supergene zone, preserved primary ores were observed in a few samples from the main deep mineralised body, which occur as residual of lenticular clusters of pyrite-magnetite-rich skarns (Figure 2A–D).

Massive pyrite (sample FLO E8) displays a gold content of about 6 g/t, as Ag-Au tellurides. It occurs as two types of habitus (Figure 2C): (i) pyrite 1 with big euhedral and

brecciated crystals (up to 5 cm) cemented by ii) finely crystallised pyrite 2. Quartz is also observed in the pyritic cement as centimetre-sized nodules and was used for the study of the paleofluids (see microthermometry results). Pyrite in this sample contains pyrrhotite inclusions and chalcopyrite associated with the Ag and Au-Ag tellurides. In another massive sulphide sample, pyrite 1 appears as relics of primary phenocrysts, intensively brecciated and cemented by chalcopyrite and covellite, followed by quartz. Malachite and chalcedony are found as late supergene alteration products.

The paragenetic sequence includes two main sub-stages (Figures 4 and 5A–D):

- Pyrite 1—arsenopyrite—(native gold).
- In a gangue made of chlorite and calcite, the following association was found: Magnetite—chalcopyrite- pyrrhotite—molybdenite—scheelite; pyrite 2—gold—sphalerite—galena—sulphosalt; telluride—native silver—native bismuth—bismuthinite. Pyrite 2 is the most abundant mineral phase.

Magnetite is abundant in the skarn and is often associated with pyrite. Magnetite also contains inclusions of pyrite, pyrrhotite, chalcopyrite, and sphalerite.

5.2. Dahapleu Prospect

In the Dahapleu prospect, the gold contents in the enclosing quartzites vary between 1.98 and 9.84 g/t. Two types of veins or associations are found (Figure 5E–H and Figure 6):

- Samples from two boreholes (SD 159 1 and 2) reveal a complex association made of quartz-tourmaline-pyrite and chalcopyrite—sphalerite—arsenopyrite—boulangerite—galena—pyrrhotite—grey copper (tennantite and tetraedrite)—native silver-gold assemblage (Figure 5E–H). No native gold was observed. However, gold combined with silver, mercury, and antimony (Figure 5H) has been detected in a grain included in chalcopyrite.
- In the other samples (SD 160 2, 164 1, 164 2, and 172), only pyrite has been observed in association with quartz and tourmaline.

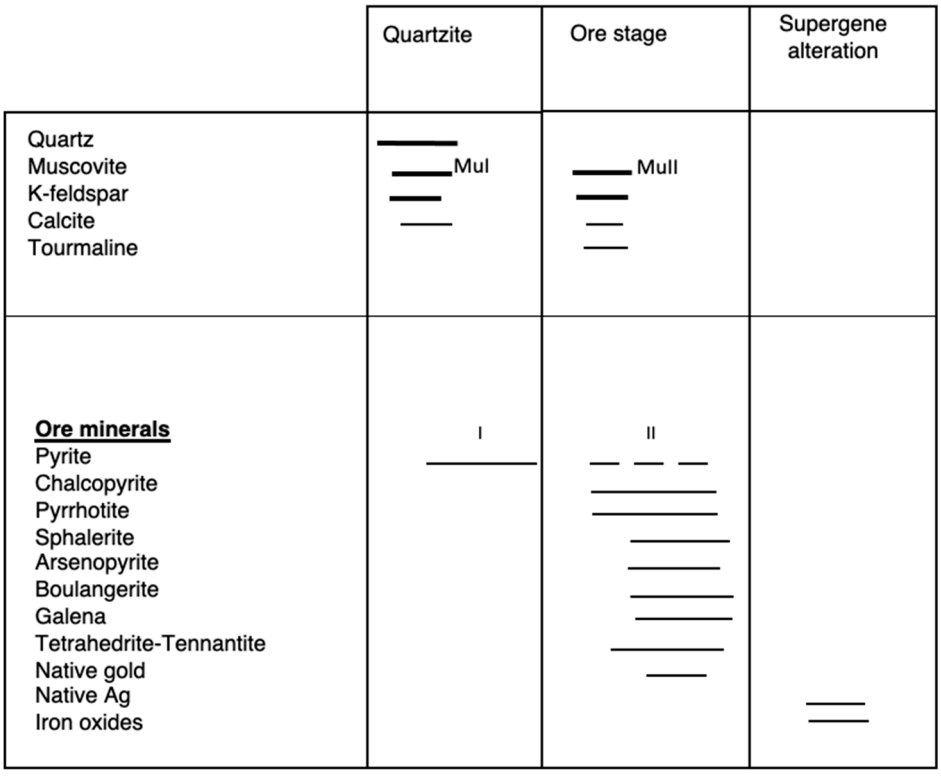

Figure 6. Paragenetic sequence of the Dahapleu gold deposit.

6. Fluid Inclusion Study

6.1. Fluid Inclusion Petrography and Types

A total of 14 doubly polished thick sections (~100 µm) were prepared from marble, sulphide-bearing quartz (Ity), garnet skarn, and Dahapleu quartzites. Over 215 fluid inclusions were examined in quartz, calcite, and garnet (Figure 7). Primary inclusions were identified by their random distribution in host minerals, whereas secondary inclusions occur along microfractures. Raman spectroscopy was conducted on 21 representative inclusions. Considering the petrographic characteristics of fluid inclusions and their microthermometric behaviour, the fluid inclusions in the Ity and Dahapleu mineralised quartz, as well as in calcite and garnet, can be divided into two main types (Table 2, Figures 7 and 8).

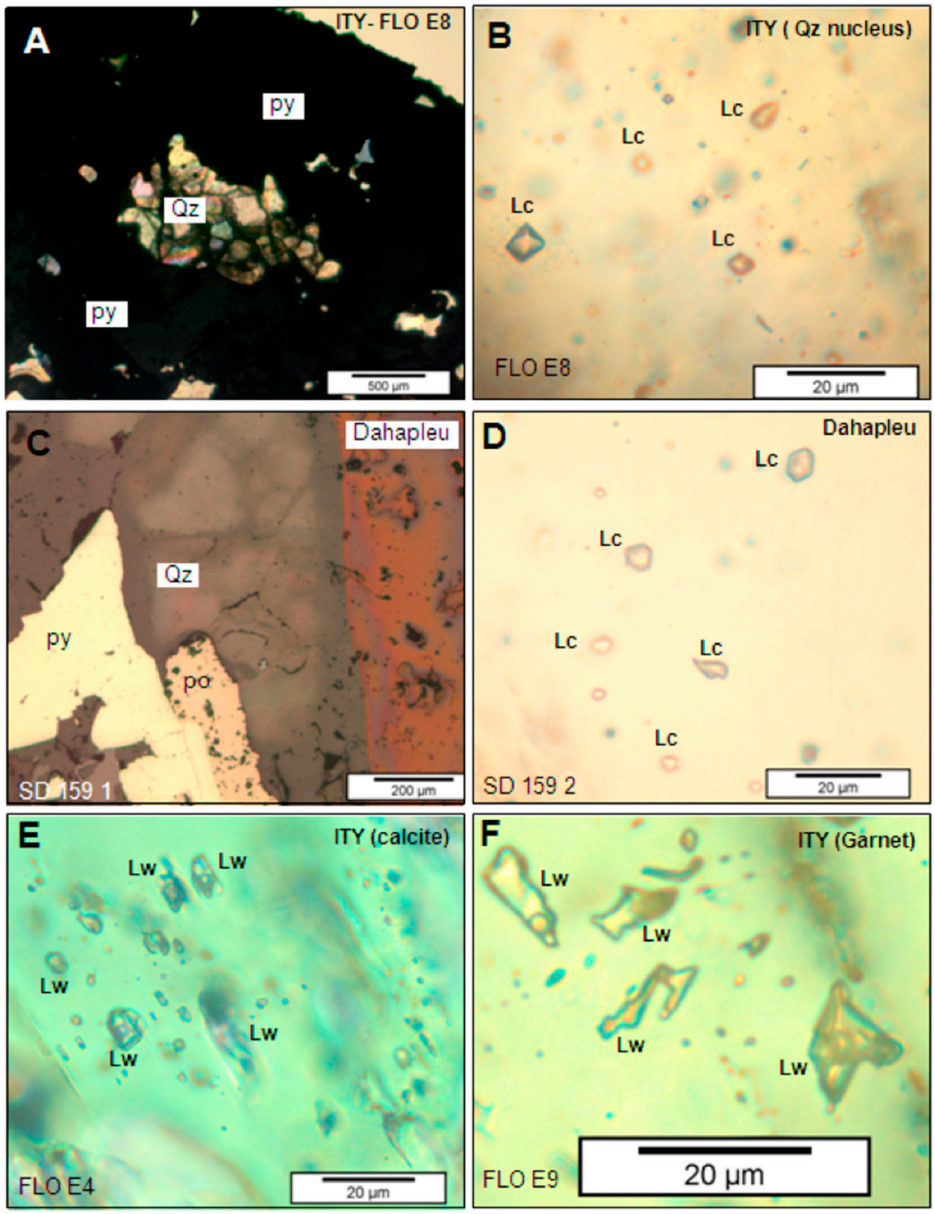

Figure 7. Main characteristics of the fluid inclusions in the Ity deposits and Dahapleu prospect. (**A**) Aspect of the quartz nucleus in the massive pyrite from Ity. (**B**) Primary carbonic fluid inclusions (Lc) in the quartz nucleus. (**C**) Studied quartz–pyrite–pyrrhotite association. (**D**) Primary carbonic fluid inclusions (Lc) observed in the Dahapleu quartz. (**E**) Cluster of primary aqueous fluid inclusions (Lw) in calcite of the enclosing marble. (**F**) Cluster of primary aqueous fluid inclusions (Lw) in garnet of the enclosing skarn.

Table 2. Summary of the microthermometric data of the different fluid inclusion types observed in the minerals from the Ity deposit and Dahapleu prospect.

Location	Sample	Mineral	Fluid Inclusions	Microthermometry			
			Aqueous-carbonic FI	***Type***	***TmCO$_2$ (°C)***	***ThCO$_2$ (°C)***	***Mode***
Flotouo	FLO E8	Quartz	Primary	c	−65.6/−58.3; n = 38	−36.5/4.6; n = 38	L
Dahapleu	SD 159 1	Quartz	Primary	c	−62/−60.5; n = 16	−15.9/0; n = 16	L
Dahapleu	SD 159 2	Quartz	Primary	c	−74.2/−59.4; n = 29	−53.5/−9; n = 29	L
Dahapleu	SD 160 1	Quartz	Primary	c	−62/−57.1; n = 31	−10.1/24.5; n = 31	L
Dahapleu	SD 164 1	Quartz	Primary	c	−57.1/−56.7; n = 24	−12.1/18.6; n = 24	L
Dahapleu	SD 164 1	Quartz	Secondary	c	−57.1/−56.9; n = 16	1.7/17.8; n = 16	L
Dahapleu	SD 172 1	Quartz	Primary	c	−58.2/−57.7; n = 23	12.2/21.6; n = 23	L
			Aqueous FI		***Tm ice (°C)***	***Th (°C)***	
Flotouo	FLO E4	Calcite	Primary	w	−19.1/−17.3; n = 5		
Flotouo	FLO E9	Garnet	Primary	w	−8.2/−4.6; n = 23	198/231; n = 12	L
Flotouo	FLO E8	Quartz	Secondary	w	0/−1.3; n = 3		
Flotouo	FLO W3	Calcite	Primary	w	−9.6/−4; n = 3		

w: aqueous inclusions; c: carbonic inclusions; n indicates the number of measurements; TmCO$_2$ melting temperature of solid CO$_2$; ThCO$_2$: homogenisation temperature of CO$_2$; Tm ice: melting temperature of ice; Th: homogenisation temperature of H$_2$O; L: Liquid. FI: Fluid Inclusions.

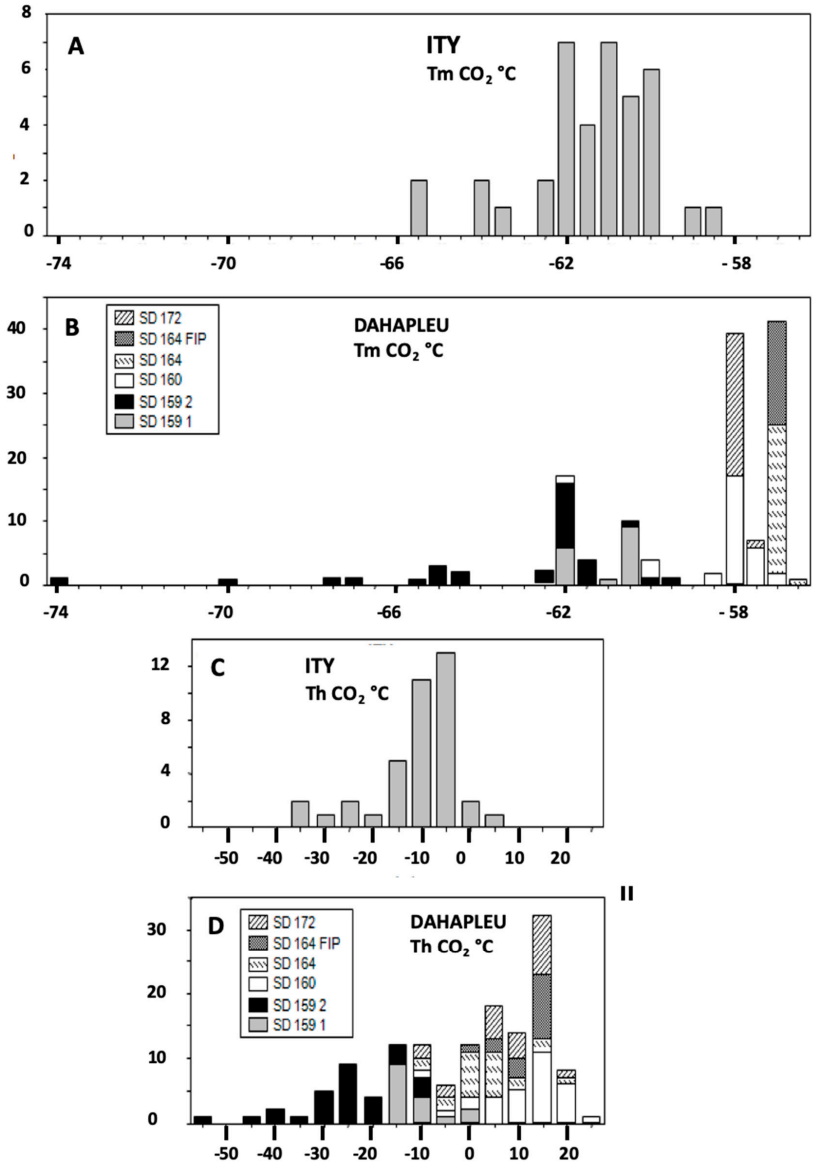

Figure 8. Histograms of melting temperature of CO$_2$ (TmCO$_2$) and homogenisation temperature of CO$_2$ (ThCO$_2$) for carbonic inclusions from Ity (**A**,**C**) and Dahapleu (**B**,**D**). In the histograms, the different captions refer to the samples mentioned in the inset.

(i) The carbonic inclusions (Lc, Figure 7B,D) belonging to the CO_2-CH_4-N_2 system occur in all types of studied quartz, generally as primary fluid inclusions and in rare cases as fluid inclusion planes (FIP). They constitute the most abundant fluids (>90%) in all the gold-bearing quartz. They have not been observed in the other minerals (calcite and garnet; Table 3).

Table 3. Chemical compositions obtained by Raman spectroscopy of selected carbonic fluid inclusions and corresponding microthermometric data from the gold-bearing quartz in the Ity and Dahapleu deposits.

Inclusion	Typology	*Microthermometry*			Raman Data (mol.%)				
		$TmCO_2$	$ThCO_2$		CO_2	CH_4	N_2	C_2H_6	H_2S
Ity									
FLO E8a	Primary	−58.9	−2.1	L	93	6.8	<0.5	nd	nd
FLO E8b	Primary	−63.4	−18.5	L	74	26	<0.5	nd	nd
FLO E8c	Primary	−64.1	−28.9	L	70	30	<0.5	nd	nd
FLO E8d	Primary	−64.2	−24.3	L	68	31.5	<0.5	<0.1	nd
FLO E8e	Primary	59.9	−4.6	L	91	9	<0.5	<0.1	<0.1
FLO E8f	Primary	−65.6	−36.5	L	62	38	<0.5	nd	nd
SD 159 1a	Primary	−62	−14	L	73	9.5	17.5	<0.1	nd
Dahapleu									
SD 159 1b	Primary	−60.6	0	L	85	5	10	<0.1	nd
SD 159 2a	Primary	−61.7	−20.6	L	76.3	9.5	14	0.2	nd
SD 159 2b	Primary	−70.1	−47.1	L	69.5	29	1	0.3	<0.1
SD 159 2c	Primary	−67.3	−39	L	38.5	59.3	1.5	0.7	<0.1
SD 159 2d	Primary	−60.5	−9	L	86.8	12	1	0.2	nd
SD 159 2e	Primary	−74.2	−53.5	L	44.8	53.6	1	0.6	<0.1
SD 160 1a	Primary	−58	15.6	L	96	3	1	<0.1	nd
SD 160 1b	Primary	−57.2	6.1	L	98.5	<0.5	1.5	nd	nd
SD 164 1a	Primary	−56.9	7.4	L	99	<0.5	1	nd	nd
SD 164 1b	Primary	−56.9	−0.7	L	99	<0.5	1	nd	nd
SD 164 1c	FIP	−57.2	17.8	L	98	<0.5	2	nd	nd
SD 164 1d	FIP	−57.1	14.1	L	98	<0.5	2	nd	nd
SD 172 1a	Primary	−57.7	6.9	L	97.5	<0.5	2.5	nd	nd
SD 172 1b	Primary	−58.2	−12.2	L	97	<0.5	<0.5	nd	nd

$TmCO_2$: melting temperature of solid CO_2; $ThCO_2$: homogenisation temperature of CO_2; L: Liquid; nd: not detected. All temperatures are in °C, FIP: Fluid inclusion plane.

(ii) Aqueous (H_2O-NaCl) fluid inclusions (Lw, Figure 7E,F) were observed in calcite and garnet minerals from marbles and skarns at Ity. They occur as primary inclusions and constitute the single fluid in these minerals. The gold-bearing quartz from Ity and Dahapleu contains a few studyable aqueous inclusions occurring in healed microfractures (sample SD 164 2).

6.2. Fluid Inclusion Data

Histograms of microthermometric results are presented in Figure 8 and Table 2 for Ity and Dahapleu, and the corresponding Raman spectroscopy data are shown in Figure 9 and Table 3.

6.2.1. The Carbonic Fluids

- In Ity, gold-sulphide bearing quartz: Primary (Lc) liquid fluid inclusions are monophase, generally dark, and do not show any visible aqueous phase at room temperature (Figure 8A–C). They are abundant (up to 90%). The melting temperature of CO_2 ($TmCO_2$) ranges from −58.3° to −65.6 °C with a maximum between −60° and –62 °C (Figure 8A). Such melting temperatures of CO_2, lower than the pure CO_2 melting point (−56.6 °C), indicate the presence of additional species such as N_2 and CH_4, as confirmed by Raman results. The homogenisation of CO_2 ($Th\ CO_2$) occurs in the liquid phase in the range −36.5° to 4.5 °C (Figure 8C). Raman analysis of 6 selected fluid inclusions shows that CO_2 is the main component of the volatile phase and is always higher than 62 mol.% (Table 3). CH_4 content ranges from 6.8 to 38 mol.%, the highest values being measured in the inclusions having the lowest CO_2 homogeni-

sation temperature. Nitrogen is always detected, but in minor amounts (<0.5 mol%) (Figure 9A). Traces of C_2H_6 (<0.1 mol.%) and H_2S (<0.1 mol.%) have been detected in a few inclusions. The volatile phase has a density ranging from 0.68 to 0.86 g/cm^3 (Figure 9B).

- In the Dahapleu gold-bearing quartz, abundant primary (Lc) predominantly monophase liquid fluid inclusions were observed in quartz from all samples (Figure 8B–D). They represent up to 99% of the fluid inclusions in that quartz. $TmCO_2$ ranges from −56.7° to −74.2 °C (Figure 8B) with a mode around −57/−58 °C, $ThCO_2$ from −53.5° to 24.5 °C (to the liquid phase; Figure 8D). Raman analysis of 13 selected inclusions (Table 3) shows that the volatile phase of these fluid inclusions contains mainly CO_2 (38–99 mol.%), with various amounts of CH_4 (0.5 to 59.3 mol.%) and N_2 (0.5 to 17.5 mol.%) (Figure 9A). Traces of C_2H_6 (<0.7 mol.%) and H_2S (<0.1 mol.%) have been observed. Estimated densities of the volatile phase range from 0.4 to 0.96 g/cm^3 (Figure 9B).

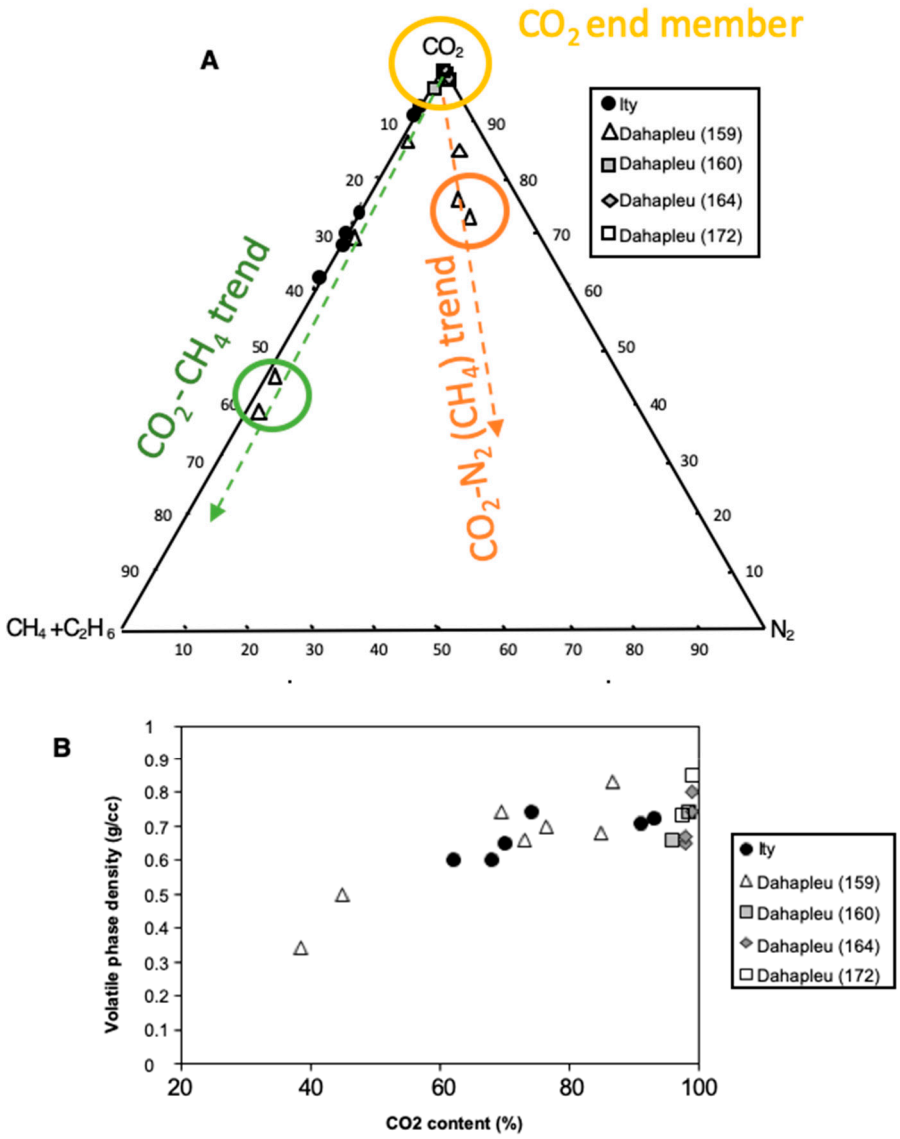

Figure 9. Composition of the carbonic inclusions. (**A**)—CO_2–N_2–CH_4+C_2H_6 ternary plot. (**B**) Density of the volatile phase versus CO_2 content diagram.

The volatile phase composition and the CO_2 phase transitions vary according to the sample location (borehole, Table 3), making it possible to distinguish between the two following groups:

(i) The samples from borehole SD 159, where fluid inclusions have the lowest homogenisation and melting temperatures of CO_2 (−59.4 °C< Tm CO_2 <−74.2 °C; –53.5 °C < Th CO_2 < 0 °C). The volatile phase of these inclusions exhibits a lower content of CO_2, ranging from 38.5 to 86.6 mol%, and CH_4, from 5 to 59.3 mol%. Variable amounts of N_2 (1 to 17.5 mol%) and traces of C_2H_6 (<0.1 to 0.7 mol%) and H_2S (<0.1 mol%) are also present.

(ii) The fluid inclusions from the other boreholes (SD 160, 164, and 172) show higher TmCO_2 (−56.7 °C to −62 °C) and Th CO_2 between −12 °C and 24,5 °C (all to the liquid phase). The volatile phase is dominated by CO_2 (96 to 99 mol.%), with very minor amounts of CH_4 (<0.5 to 3 mol.%) and N_2 (<0.1 mol.%) (Figure 9). Traces of C_2H_6 (<0.1 mol.%) have been detected in only one inclusion.

Secondary (Lc) monophase liquid inclusions have been observed only in sample SD 164 1. Tm CO_2 are in the range −56.9 °C to −57.1 °C. CO_2 homogenises into the liquid phase in the range of −1.7 °C to 17.8 °C. Raman analysis of the two selected inclusions (Table 3) shows that the volatile phase is dominated by CO_2 (98 mol.%), with small amounts of N_2 (2 mol.%) and a very low quantity of CH_4 (<0.5 mol.%). This composition is similar to that obtained in the primary carbonic fluid. Estimated densities of the volatile phase of secondary (Lc) monophase liquid inclusions are all around 0.8 g/cm3.

The CO_2–N_2–CH_4+C_2H_6 ternary plot indicates that most fluids distribute between two end-members: a fluid close to pure CO_2 and a fluid with methane amounts reaching 60%. The presence of N_2 is significant in a smaller number of inclusions from Dahapleu. The volatile density decreases from the CO_2-rich end-member towards the fluid richer in methane.

6.2.2. The Aqueous Fluids

- At the Ity deposit, primary (Lw1) aqueous inclusions were observed in both calcite (sample FLO E4, W3) and garnet (sample FLO E9) (Figure 7E,F). They constitute the only fluids observed in these samples. The melting temperature of ice (Tm ice) is observed between −19.1 °C and −4 °C; the lowest (−19.1 °C to –17.3 °C) is in sample FLO E4. The homogenisation temperature (Th) occurs to the liquid phase in the 198 °C to 231 °C range. The estimated salinities range from 6.5 to 21.7 wt% % eq. NaCl. Rare secondary (Lw2) two-phase aqueous inclusions occur in the Ity sulphide-gold bearing quartz (sample FLO E8). Tm ice ranges from 0 and −1.3 °C, corresponding to a salinity ranging from 0 to 2.2 wt% eq. NaCl, and Th is around 150 °C.

7. Discussion

7.1. Pressure–Temperature Interpretation

Representative isochores were calculated for each type of fluid by considering results from microthermometry and Raman analysis. The derived chronological reconstruction is shown on a pressure versus temperature plot (Figure 10). The pressure–temperature estimates considered at the different stages of the P-T path are as follows: (i) the peak of metamorphism conditions for the Eburnean orogeny at 500 to 650 °C and 500 to 600 MPa [45]; (ii) the retrograde greenschist facies conditions of Birimian rocks hosting gold mineralisation were <450 °C and <300 MPa, [45]; (iii) the retrograde evolution of D2 metamorphism phase in Toulepleu–Ity region, from 600 °C and 400 MPa to 580 °C and 280 MPa [34]; (iv) the Ity mineralising temperature estimates deduced from petrographic and mineralogical features [16], are in the range 500 to 600 °C.

7.1.1. Early Stages

Due to the similarities in the association and nature of carbonic fluid inclusions and secondary aqueous inclusions at the two locations, data from the Ity deposits and Dahapleu prospect are discussed together in the following paragraph. The primary aqueous inclusions are absent in the quartz, whereas they represent the only fluid inclusions in calcite (marble) and garnet (skarn). Their salinity is generally high, reaching 22 wt% eq. NaCl. Fluids associated with Au skarns worldwide are usually of high salinity [46–54]. However, these fluids cannot represent the mineralising fluids because: (i) the aqueous fluid inclusions have not been observed in the quartz core enclosed in the mineralised samples; (ii) they are observed as primary fluid inclusions in calcite from the marbles, which have formed before ore deposition. An estimation of the skarn formation conditions during syn-D2 intrusions (around 2100 Ma) was proposed by Triboulet and Feybesse [34] for the Ity area (Figure 10A). This corresponds to the later stage of the retrograde P-T path, evolving from the D1 amphibolite-facies deformation stage to conditions associated with granitic intrusions (D2).

Retrograde metamorphic paths in this region of West Africa vary according to the metamorphic domains and terranes, as illustrated by [55] for Ghana, where three characteristic paths are depicted (see Figure 10A,B). However, the nature of parageneses in the host rocks at Ity, along with the geological history proposed by Triboulet and Feybesse [16], suggests that the Ity zone was most likely affected by a high-pressure drop trajectory, with temperatures decreasing from 650 to 550 °C, thus a rather significant drop in pressure, not isothermal, but occurring with a relatively high temperatures suggesting the exhumation of a hot lithospheric block at a rather high structural level with a deficit in the thermal re-equilibration (Figure 10A). This trajectory evolved from amphibolite-facies conditions at pressures exceeding 500 MPa (D1 stage, approximately 500–800 MPa, around 2130 Ma) and is similar to the P-T path for amphibolite facies series from [55] (Figure 10B).

The fact that intrusions during D2 formed in this abnormally hot zone is coherent and may be very important for the following episodes, and may indicate quick exhumation of high-T terranes.

7.1.2. Gold Stage

The exhumation, which is, on the reverse of the preceding path, strongly anisothermal at sub-constant pressure, may indicate that the hot spot began to cool, in particular during deformation. At that stage, fluid movements in shear zones could have contributed to the accelerated cooling thanks to convection around the hot spot. Additionally, the fluid movements could have leached source rocks and mobilised metals. The skarn location is therefore indicative not only of a passive boundary between granite and its enclosing metasedimentary units but also of the locus of a hot spot, as in the case of many other deposits where a succession of favourable factors concentrates around the exact location.

At that stage, the carbonic inclusions are the most abundant in quartz associated with massive sulphides (Ity deposit) and quartz from quartzites (Dahapleu), but are absent in calcite and garnet. The quartz cores in the massive sulphide contain predominantly primary CO_2-CH_4-N_2 fluid inclusions. The gas mixtures with no visible aqueous phase are mainly composed of CO_2 (62–93 mol.%), CH_4 (6.8–38 mol.%), with minor amounts of N2 (<0.5 mol.%). Its estimated density is high (a range between 0.6 and 0.8 g/cm^3). Several features suggest that these CO_2-CH_4 $\pm$ N_2 fluid could represent the mineralising fluids or at least have play a role in the mineralising process: (i) the primary setting of the gaseous fluid inclusions in clusters and intragranular trails; (ii) the inclusions are well shaped and do not show post-entrapment features; (iii) the remarkable absence of brine fluid inclusions in quartz.

The second remarkable feature in the studied area is the substantial differences between the fluid compositions and densities in the Dahapleu prospect and the Ity skarn. At Ity, fluids are predominantly rich in CO_2, with a relatively small density range. In the Dahapleu shear zone, a large variety of fluids was found, which indicates a series of fluid trapping events of contrasting compositions. Their density does not show an extensive range, although it is slightly wider than in Ity samples. At reverse, the sample 159 from Dahapleu exhibits a vast range of fluid compositions and densities, indicative of distinct fluid trapping: fluids rich in CH_4, and fluids with compositions close to those of Ity, but with a more extended trend towards the CH_4 end-member, and a series of fluids with both CO_2, CH_4 and N_2 defining a second trend in direction of a N_2 end-member. Secondary fluids are dominated by CO_2 (sample 164).

As a conclusion, volatile phase composition describes mixing trends between three end-members: a CO2-rich fluid, a CO_2-CH_4 end-member, and a CO_2-N_2 end-member. Such contrasted compositions cannot be issued from simple unmixing and are further evidence of the fluid production within the metamorphic series. CH_4 is generally attributed to lower redox conditions, and devolatilisation of the C-rich matter and water-graphite equilibria [56], and N_2 may be released from the oxidation of ammonium present in micas.

7.1.3. Origin of the CO_2 Dominated Inclusions

Single-phase liquid inclusions at room temperature, which homogenise to a single liquid phase (L), such as those observed at Ity, have also been reported from gold deposits in the Ivory Coast (Angovia; [57], Ghana (Ashanti) [58–62], and Burkina Faso [63]. Numerous studies have described and debated the significance of these fluid inclusions, which are frequently observed in mineralised quartz or along the margins of auriferous veins [5]. Specific debates about the nature of the mineralising fluid and the significance of the fluid inclusions occurred in the years 1996–2004 on the case of the Ghana deposits, and in particular the Ashanti belt: [59,61,62,64,65]; summary of previous works in [66].

The interpretation of the predominance of CO_2-dominated inclusions has been highly debated, with two end-member views. In the first concept, the fluid unmixing hypothesis, CO_2-dominated inclusions are considered primary evidence of immiscibility in a mixed H_2O–CO_2 system during mineralisation. Their coexistence with aqueous inclusions in the same growth zones supports phase separation as a mechanism for destabilising gold complexes and triggering precipitation. In this model, CO_2 plays an active though indirect role in ore formation, and unmixing is viewed as a critical ore-forming process in Birimian systems [59,67]. In the second concept, the "post-entrapment modification hypothesis", CO_2-dominated inclusions may be artefacts of post-trapping modification. During plastic deformation of quartz, selective leakage of H_2O can enrich inclusions in CO_2, producing "apparent" CO_2-only inclusions not representative of the original fluid [65,68,69]. In this scenario, the proper and mineralising fluid was a low-salinity H_2O–CO_2 mixture of metamorphic origin, and the apparent abundance of pure CO_2 inclusions reflects re-equilibration during deformation, rather than fluid unmixing. Evidence exists in support of both models: some Birimian deposits preserve textural relationships compatible with primary fluid immiscibility, while in others microstructural criteria favour secondary modification. This duality underlies the long-standing controversy: CO_2-dominated inclusions may either represent a key stage of ore fluid evolution or a misleading artefact of deformation-related re-equilibration.

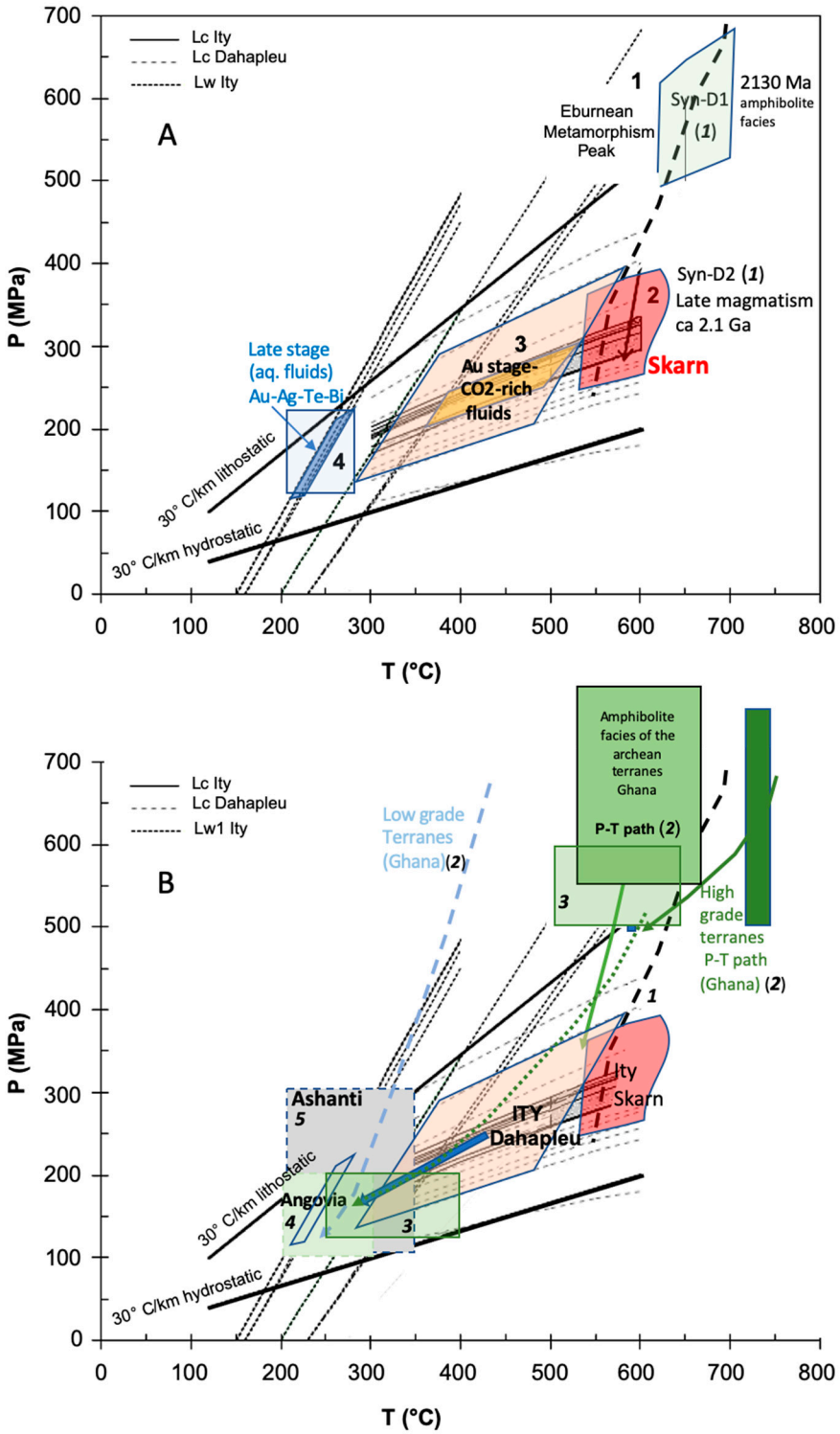

Figure 10. (**A**) General pressure–temperature diagram of the conditions prevailing in the Ity area. 1: Peak metamorphism conditions for Eburnean orogeny [34]; 2: Retrograde evolution during D2 tectonism in Toulepleu–Ity unit down to the granite intrusion and skarn formation [34], the dashed black line summarises the retrograde trend from [34]; 3: conditions of gold mineralisation at Ity constraining the pressure from CO_2-rich fluid inclusions; 4: late stage and aqueous fluid inclusions. (**B**) Regional comparisons: 2: three P-T paths proposed for different lithologies and terranes in Ghana [55], 3: the P-T path (green dashed line) proposed by [45] for Ashanti area with two boxes for the highest and lowest P-T conditions; 4: the P-T bow for the formation of the Angovia deposit [57]; 5: P-T box for the Ashanti gold area by [59].

In the studied Ity and Dahapleu area, there is no evidence of fluid unmixing, and the quartz included in sulphides at Ity is not deformed. Therefore, the alternative is to propose that CO_2-rich fluids with low water content and variable CH_4 or N_2 contents were issued from the water–rock interactions within metasedimentary formations. A key issue lies in the accurate determination of water content, which is often constrained by observational limits: the resolving power of standard petrographic microscopes is insufficient to detect menisci only a few microns in size—yet such undetected volumes could correspond to over 5–10 mol% of invisible molecular water. This water amount associated with volatile fractions potentially containing ligands, such as H_2S or HS^- in amounts not detectable by Raman spectroscopy, could have extracted gold from favourable source rocks, as most crustal fluids are undersaturated with respect to gold.

7.1.4. Relationships Between Gold, Skarn, Shear-Zones, and P-T Evolution

Most authors interpret the CO_2-rich fluid inclusions as evidence of metamorphic fluids derived from the dehydration of crustal rocks, which are enriched in CO_2 through the decarbonation of carbonates or the assimilation of carbon-rich sedimentary material. These fluids are thought to have migrated along major fault systems under transpressive regimes during Birimian deformation episodes. It remains uncertain whether the high-salinity inclusions associated with the skarn stage persisted during the later migration of aqueous-carbonic fluids. However, in gold-bearing quartz, CO_2-rich fluids are not associated with high-salinity brines or low-salinity aqueous inclusions (H_2O–NaCl).

For stages following intrusion and skarn formation, the spatial association between gold mineralisation and shear zones—particularly in the Dahapleu area—supports hypotheses that gold concentration is linked to a subsequent deformation stage (possibly D3). The attribution of the gold phase event to the D3 deformation event is logical, but has not yet been supported by a direct geochronological approach. Accurate dating of minerals from the gold assemblage will be the future challenge to fully understand and develop a comprehensive conceptual model of the mineralisation process.

Trapping pressures for fluid inclusions at Ity can be, however, relatively well constrained, assuming that the inclusions were not significantly affected by post-entrapment modifications. The associated isochores are relatively flat, meaning they are not strongly temperature-dependent, allowing for the estimation of trapping pressures in the range of 200 to 300 MPa (Figure 10A). These pressure conditions are typical of the brittle–ductile transition zone and are consistent with gold deposition settings, although slightly higher than those proposed in the literature for other deposits in Birimian terranes (Figure 10B).

Estimating temperature is more challenging due to the lack of reliable mineralogical markers directly associated with the early stage of gold precipitation. Thus, silicate mineral assemblages provide few reliable constraints for the gold deposition stage, except for the fact that chlorite and epidote are stable over a relatively large range of temperatures from 200 to 390 °C. The temperature range for the gold stage is thus constrained between the upper limit for skarn formation (450–550 °C) and the lowest values of 200 °C attributed to the late assemblages (Bi-Bi-tellurides, Au-Ag tellurides: 140–270 °C). From the study of many other metamorphic quartz, the CO_2-CH_4-H_2O fluids are generally formed by graphite-water equilibrium above 350–380 °C [56,70]. Below this temperature, methane becomes the predominant volatile phase. So, it is likely that carbonic fluids were trapped close to or above the 350–380 °C window first. It cannot be ruled out that the upward trend in CH_4 may reflect not only the devolatilisation of carbon-rich units, but also the drop in temperature below 350 °C, the lowest temperature of the graphite-water equilibrium.

7.1.5. Late Stages

The secondary aqueous inclusions were observed in the mineralised quartz as fluid inclusion planes. The relatively low salinity of the late aqueous fluids (Lw2) is similar to that described in some Archean gold deposits [71–73]. Such fluids are likely attributable to the late events, as the few isochores intersect the temperature range inferred for the Au-Bi-Te association.

7.2. The Ore Formation

At Ity, the primary ores occur in a series of lenticular clusters of skarns rich in sulphides and magnetite. The epigenetic sulphide mineralisation was first considered to be contemporaneous with the contact metamorphism that produces marbles and skarn assemblages [16,74]. However, the role of later fluid circulation triggered by faults is important and overpasses the initial skarn formation. The highest gold contents were found inside and near iron-rich formations. Preconcentrations linked to the skarn stage are therefore not precluded, in particular in metals such as Cu, Mo, and W. The presence of the Dahapleu ores in faults, however, may indicate that the skarn stage is not responsible for the entire gold stock.

The precise role of CO_2 in gold precipitation remains a topic of debate. Some researchers argue that CO_2-rich fluids, due to their low polarity and limited capacity to complex gold, are unlikely to have directly caused precipitation [75]. Instead, they may represent an early transport phase as transporting other gas species such as H_2S, or act as a chemical buffer within the hydrothermal system. Others propose that gold precipitation was triggered by physical-chemical changes, such as pressure fluctuations associated with seismic valve mechanisms—an especially plausible scenario within shear zones.

The origin of CO_2 has been a subject of debate for more than three decades, based on stable isotope analyses of carbon and oxygen in gold-associated minerals and fluid inclusions [64,76,77]; see reviews by [66,78]. It remains challenging to determine whether the CO_2 could derive from deep-seated fluids of mantle or magmatic origin, especially those associated with syn-orogenic felsic intrusions. Few studies have explicitly focused on the origin of CO_2 in fluid inclusions. Among them, Lüders et al. [79] argue that in the West African Craton, CO_2 primarily results from devolatilisation of metasedimentary rocks rich in carbon and cannot be attributed to a mantle source. The presence of methane in significant amounts supports this hypothesis. It may be attributed to the equilibration of water with graphite in metasedimentary units at temperatures exceeding 500 °C—which helps explain the formation of the methane-rich fluid end-member [56]—or below 380 °C.

7.3. Fluid–Rock Interaction with Impure Marbles and Skarn Silicates: A Mechanism for Gold Complex Destabilisation

At the Ity deposit, the transition from the pyrite-bearing stage to the gold-bearing stage is marked by the widespread occurrence of pyrrhotite, replacing earlier pyrite. This mineralogical evolution is indicative of a decline in aqueous H_2S activity, which is controlled by the progressive crystallisation of iron sulphide phases during hydrothermal fluid–rock interaction. Thermodynamically, this evolution reflects a redox shift from the magnetite–pyrite buffer towards the magnetite–pyrrhotite buffer, corresponding to decreasing fO_2 and fS_2. This redox trajectory is widely recognised as a key mechanism for gold precipitation, involving the destabilisation of gold–bisulphide complexes, such as $Au(HS)_2^-$ [80].

Such redox and sulphiidation processes are particularly effective in impure marbles and carbonate-bearing metasediments that have undergone skarn alteration. These lithologies contain reactive Fe^{2+}-bearing silicates (e.g., biotite, amphibole, actinolite, feldspar)

that undergo sulphidation upon interaction with H_2S-rich fluids, leading to pyrrhotite precipitation and acidification of the fluid:

$$Fe_{(rock)}{}^{2+} + H_2S_{(fluid)} \rightarrow Fe_{1-x}S_{(po)} + 2H^+$$

This consumption of H_2S reduces sulphur activity in the fluid, destabilising gold complexes and promoting precipitation of native gold. The concurrent release of protons lowers the pH, which further contributes to the destabilisation of the complex. The CO_2 release by decarbonation during skarn formation adds another dimension to fluid modification. Experimental studies have demonstrated that increasing the CO_2 content in hydrothermal fluids decreases the stability of $Au(HS)_2{}^-$ and other gold complexes, thereby enhancing gold deposition under CO_2-rich, reduced conditions [81]. This mechanism is particularly effective in carbonate–Fe–rich silicate assemblages, where the interplay of decarbonation, sulphidation, and pH buffering creates strong chemical gradients favourable to gold deposition [82]. Impure marbles do not merely act as passive host rocks but serve as reactive geochemical barriers. The skarn associations can modulate redox state, sulphur speciation, and CO_2 content in migrating fluids, making them critical zones for gold trapping and mineralisation in skarn and orogenic gold systems.

In addition, bismuth is present during the late stages of the gold events, having been found either as native bismuth or bismuthinite, is associated with tellurides, and is frequently found in earlier magnetite nuggets. Following Zhou et al. [83], at the surface of magnetite where fO_2 is fluctuating, bismuth melt can scavenge gold. Later on, the sulphidation of bismuth can promote gold precipitation. All the players described by Zhou et al. [83] are present at Ity, where gold and bismuth phases are found as inclusions in close relation with magnetite. The most probable temperatures for these processes range from 200 to 300 °C [84].

7.4. Comparison with Other Deposits

The Ity gold deposit represents the only Birimian one spatially associated with skarns in eastern Africa. Even if most skarns are associated with Phanerozoic plutons [85,86], several skarn deposits have been described in older orogenic belts (Lucky Draw, Australia; [87]; Navachab, Namibia; [88]. Carbonate rocks are not common in the Birimian formations of West Africa [8]. Elsewhere, the marbles of the Siguiri basin in Guinea and the Dialé–Daléma series in Senegal and Mali are the most extensive occurrences of carbonate rocks in the Birimian terranes of West Africa [89–91]. However, exploration of the magnetite-rich skarn of the Dialé–Daléma series for gold was not successful. In this deposit, magnetite is associated with clinopyroxene, phlogopite, serpentine, and garnet. Sulphides consist of pyrrhotite and subordinate pyrite, chalcopyrite, arsenopyrite, pentlandite, and cobaltite [91]. In the eastern part of the Dialé–Daléma series, the Sadiola gold deposit (Mali), which is partly enclosed in carbonate rock and exhibits an arsenopyrite-pyrrhotite-pyrite-stibnite-gudmundite association, is interpreted as having a mesothermal origin [92].

7.4.1. Au Skarn Deposits

Fluid inclusion characteristics of worldwide gold skarn deposits are all dominantly aqueous fluid inclusions, characterised by high temperature and high salinity (86). Even if fluid inclusions have already provided direct evidence for the presence of CO_2, CH_4, N_2, and H_2S in the fluids of a few skarn worldwide (e.g., magnetite skarn, Falémé, Senegal; Cu-Au skarn, La Paz, Mexico), these volatile phases appear subordinate [50,86,91]. Thus, at Ity, only the early brines can be attributed to the skarn stage.

7.4.2. Quartz Vein-Type Deposits in the Birimian Terranes

Synthetic overviews of the nature of the fluid inclusions have been proposed by Konate et al. [93] and Béziat et al. [94]. The trapping temperatures and pressures of the Ashanti gold deposits in Ghana were estimated to be 220 to 440 °C and 190 to 540 MPa [61], 400 ± 50 °C and 200 to 400 kbar [95], and 370° to 470 °C at 200 MPa [58]. In Diabatou (Burkina Faso), the primary gold mineralisation occurred between 300 and 380 °C and at pressures about 300–500 MPa [96]. The two main differences concern the volatile rich inclusions from Ity and Dahapleu deposits compared to the features of inclusions from other mineralisations observed elsewhere in West Africa, are (i) the predominance of CH_4 over N_2 in the volatile phase, mainly composed of CO_2; (ii) the significantly higher temperatures estimated for the Ity and Dahapleu deposit than the other deposit. Even if the high-density CO_2-CH_4-N_2 fluids are uncommon in lode gold deposits [72,97–101], some evidence suggesting mineralisation of gold from high-density CO_2 (N_2) rich fluid in high-grade terranes of Australia, South Africa, India, and Brazil has already been established [98,102–104].

The mineralising fluids at Ity exhibit a similar nature (carbonic inclusions) to those observed in the majority of the Birimian lode gold deposits of West Africa, indicating a predominance of the mesothermal source. In addition, significantly higher trapping temperatures are supposed at the Ity deposit compared to the majority of West Africa lode gold deposits. Figure 10B shows that the P-T box for Angovia is located within lower P-T ranges than those inferred for Ity. Such temperatures could reflect the local influence of a long-lived magmatic heat source, such as the one that produced the earlier contact metamorphism. The role of skarn could nevertheless be a preconcentration stage or a primary stage from which evidences were not found or demonstrated. Frequently, significant ore deposits result from a series of events occurring at the exact location, all of which play a role in the history of metal concentration.

8. Conclusions

The Ity area permits the study of both an Au-deposit spatially related to a skarn developed by an intrusion in a metasedimentary sequence, and at Dahapleu, a skarn-free deposit, structurally controlled. The Ity skarn itself was probably initially mineralised in Cu, Mo, and W. At Ity, the mineralisation occurs predominantly within skarn bodies and quartz-rich zones, comprising a series of events: (i) an early assemblage of pyrite, arsenopyrite, and native gold; (ii) a more complex sulphide–magnetite association and finally Au-Ag-Bi-Te associations. The Dahapleu prospect exhibits many mineralogical and fluid inclusion similarities with Ity, but differs in the absence of magnetite and the presence of grey copper and boulangerite. There are therefore strong contrasts in the same area in the ore mineralogy, redox conditions and local lithologies.

Similar contrasts were found in the fluid story:

- A saline aqueous fluid (H_2O-NaCl), preserved as primary inclusions exclusively in calcite and garnet from the marbles and skarns from Ity. These fluids are interpreted as being associated with early metasomatic and contact metamorphic processes, but not directly involved in ore deposition. They are absent at Dahapleu.
- A carbonic fluid CO_2-dominated with no visible water, preserved as abundant, primary monophase (liquid) inclusions in quartz associated with gold mineralisation, both at Ity and Dahapleu. The volatile content of these defines two mixing trends, a predominant trend towards a CH_4 end-member (up to 59 mol.%) and a second trend towards a N_2-enriched (CO_2-CH_4) end-member. Fluid densities are high (0.8 ± 0.1 g/cm^3). The absence of such carbonic fluids in calcite and garnet further supports their temporal and genetic link with the gold-bearing event.

Several lines of evidence indicate that the carbonic fluids represent, or at least closely record, the ore-forming fluids: their primary inclusion textures and intragranular occurrence; their spatial association with gold and sulphide phases; and the absence of aqueous fluids in the ore-bearing quartz, except for a few secondary fluid inclusions. The gold preconcentration during the early stages of skarn formation is not precluded, but the following steps are probably critical for the formation of the primary ores. The specific location of the Ity deposit, in close association with the skarn, could have benefited from the presence of iron-rich assemblages (silicates, magnetite), which may have triggered, later on, the precipitation of sulphide, in turn favouring gold enrichments. The bismuth brought by the late circulating fluid could also have played a role in scavenging gold.

The mineralising system at Ity, although spatially related to skarn, exhibits fluid inclusion features more typical of mesothermal orogenic gold systems, probably hotter than in other West African Birimian deposits. The Ity deposit formed consequently through a hybrid model: a mesothermal orogenic gold system dominated by CO_2–CH_4 fluids at >350 °C, superimposed on earlier skarn mineralisation. This direct and tangible evidence from the study of paleofluids complements previous models proposed for both Ity and the Birimian gold mineralisations.

This study highlights the importance of integrating fluid inclusion microanalysis and paragenetic reconstruction to better constrain the hydrothermal evolution that contributes to gold mineralisation in the Paleoproterozoic domains of West Africa. Future challenges are the following: (i) the direct dating of the mineralising event to confirm the gold event to the D3 deformation; (ii) the search of fluid and metal sources; (iii) a better understanding of the causes of long-lived thermal systems, as revealed by a succession of several favorable events at the exact location, including a quick exhumation of hot lithospheric crust; such events are followed by granite intrusion and skarn formation, and then shear deformation. Additional work on this type of deposit may also concern metals present in trace amounts in the same rock volume due to the complex succession of mineralising events. The enrichment of co-products (Bi-Te, W, Cu) is indeed one of the objectives of the responsible mining industry for the future.

Author Contributions: Conceptualisation, Y.C. and M.-C.B.; methodology Y.C. and M.-C.B.; validation, Y.C., M.-C.B. and M.C.; Y.C. investigation, M.-C.B., resources, Y.C. and M.-C.B.; data curation, Y.C., M.-C.B. and M.C.; writing—original draft preparation, Y.C. and M.-C.B., writing—review and editing, M.C., project administration, Y.C.: funding acquisition, Y.C. and M.-C.B. All authors have read and agreed to the published version of the manuscript.

Funding: This study was financially supported by EGIDE (French cooperation agency), thanks to the Cultural Service from the French Embassy in Abidjan and MC Marchal from EGIDE (Nancy), for Y. Coulibaly's stay in Nancy at UMR 7566 (G2R). CREGU has assumed responsibility for the analytical fees.

Data Availability Statement: Data are available on request to the authors.

Acknowledgments: The Authors express their sincere gratitude to Philippe Palanque and Pol Urien, Société des Mines d'Ity, for their assistance in accessing the Ity open pit during sampling and for their discussions about the Ity geology. R. Mathieu is acknowledged for his help in providing technical data and maps. Thérèse Lhomme is thanked for her help during the Raman analysis. Two anonymous reviewers are warmly acknowledged for their suggestions and pertinent remarks, which significantly improved the manuscript.

Conflicts of Interest: The authors declare that they have no conflicts of interest.

References

1. Lawrence, D.M.; Allibone, A.H.; Chang, Z.; Meffre, S.; Lambert-Smith, J.S. The Tongon Au deposit, northern Côte d'Ivoire: An example of Paleoproterozoic Au skarn mineralisation. *Econ. Geol.* **2017**, *112*, 1571–1599. [CrossRef]
2. Le Mignot, E.; Reisberg, L.; André-Mayer, A.-S.; Bourassa, Y.; Fontaine, A.; Miller, J. Re-Os geochronological evidence for multiple Paleoproterozoic gold events at the scale of the West African craton. *Econ. Geol.* **2017**, *112*, 145–168. [CrossRef]
3. Masurel, Q.; Eglinger, A.; Thébaud, N.; Allibone, A.; André-Mayer, A.S.; McFarlane, H.; Miller, J.; Jessell, M.; Ailleres, L.; Vanderhaeghe, O.; et al. Paleoproterozoic gold events in the southern West African Craton: Review and synopsis. *Miner. Depos.* **2022**, *57*, 513–537. [CrossRef]
4. Ouattara, Z.O.; Coulibaly, Y.; Boiron, M.-C. Shear-hosted gold mineralisation in the Oumé-Fettèkro belt, Côte d'Ivoire: The Bonikro deposit. *Geol. Soc. Lond. Spec. Publ.* **2021**, *502*, 147–158. [CrossRef]
5. Ouattara, Z.; Gouédji, G.F.E.; Allialy, M.E.; Monouin, P.J.C.; Coulibaly, Y. Mineralization and sustainable development in the West African Craton: From field observations to modelling. *J. Geosci. Geomat.* **2022**, *10*, 153–161.
6. Salvi, S.; Aponsah, P.O.; Siebenaller, L.; Béziat, D.; Baratoux, L.; Jessell, M. Shear-related gold mineralisation in northwest Ghana: The Julie deposit. *Ore Geol. Rev.* **2016**, *78*, 712–717. [CrossRef]
7. Milési, J.P.; Feybesse, J.L.; Ledru, P.; Domanget, A.; Ouédraogo, M.F.; Marcoux, E.; Prost, A.E.; Vinchon, C.; Sylvain, J.P.; Johan, V.; et al. Les minéralisations aurifères de l'Afrique de l'Ouest. Leurs relations avec l'évolution lithostructurale au protérozoïque inférieur. *Chron. Rech. Min.* **1989**, *497*, 3–98.
8. Milési, J.P.; Ledru, P.; Feybesse, J.L.; Domanget, A.; Marcoux, E. Early Proterozoic ore deposits and tectonics of the Birimian orogenic belt, West Africa. *Precambrian Res.* **1992**, *58*, 305–344. [CrossRef]
9. Kusnir, I. Gold in Mali. *Acta Montan. Slovaca* **1999**, *4*, 311–318.
10. Thébaud, N.; Allibone, A.; Masurel, Q.; Eglinger, A.; Davis, J.; André-Mayer, A.S.; Miller, J.; Ouedrago, M.F.; Jessell, M. The Paleoproterozoic (Rhyacian) Gold Deposits of West Africa. In *Geology of the World's Major Gold Deposits and Provinces*; Sillitoe, R.H., Goldfarb, R.J., Robert, F., Simmons, S.F., Eds.; Society of Economic Geologists: Littleton, CO, USA, 2020; pp. 735–752.
11. Perret, J.; Jessell, M.; Masurel, Q.; Hayman, P.C.; Thébaud, N.; Baratoux, L.; Kouamélan, A.; Eglinger, A.; André-Mayer, A.S.; Koffi, A.Y.; et al. Review of Paleoproterozoic tectonics in the southern West African Craton: Insights from multi-disciplinary data integration. *Precambrian Res.* **2025**, *422*, 107707. [CrossRef]
12. Naho, J. Cycle Supergène De L'or En Milieu Ferralitique. Exemple du Gisement D'or D'ity En Côte d'Ivoire. Unpublished Ph.D. Thesis, Institut National Polytechnique de Lorraine, Nancy, France, 1988; 132p.
13. Granier, C.; Lajoinie, J.-P.; Vitali, C. Géochimie de l'or et du cuivre dans les formations latéritiques argileuses du Mont Flotouo (Ity, Côte d'Ivoire). *Bull. Soc. Franç. Minér. Crist.* **1963**, *LXXXVI*, 253–258. [CrossRef]
14. Béziat, D.; Feybesse, J.-L.; Ledru, P.; Dommanget, A.; Ouedraogo, M.-F. A weathered skarn-type mineralisation in Ivory Coast: The Ity gold deposit. *J. Afr. Earth Sci.* **2015**, *112*, 524–535.
15. Mathian, M.; Hebert, B.; Baron, F.; Petit, S.; Lescuyer, J.L.; Furic, R.; Beaufort, D. Identifying the phyllosilicate minerals of hypogene ore deposits in lateritic saprolites using the near-IR spectroscopy second derivative methodology. *J. Geochem. Explor.* **2018**, *186*, 298–314. [CrossRef]
16. Lajoinie, J.P.; Fonteilles, M. Un gîte de skarns latéritisés: Le gîte aurifère d'Ity (Côte d'Ivoire). In *Chronique des Mines d'Outre-mer*; Bureau d'Etudes géologiques et minières: Orléans, France, 1968; Volume 378, pp. 143–153.
17. Yacé, I. *Le Précambrien de L'afrique de l'Ouest et ses Corrélations Avec le Brésil Oriental*; Rap Final du Projet PICG; CIFEG, publ. Occas.: Orléans, France, 1984; Volume 2, 28p.
18. Bessoles, B. Géologie de l'Afrique: Le craton ouest-africain. *Mém. BRGM* **1977**, *88*, 259–262.
19. Kouamélan, A.N. *Geochronologie et Geochimie des Formations Archeennes et Proterozoïques de la Dorsale de Man en Cote D'ivoire*; Géosciences Univ. Rennes: Rennes, France, 1996; Volume 73, 289p.
20. Tagini, B. Esquisse Structurale De La Cote D'ivoire. Essai de Geotectonique Regionale. Unpublished Ph.D. Thesis, Lausanne University, Lausanne, Switzerland, 1971; p. 302.
21. Tysdal, R.G.; Thorman, C.H. *Geological Map of Liberia, 1/1000000 Map 1–1480*; Ministry of Land and Mines, Liberia Geol. Surv.: Monrovia, Liberia, 1983.
22. Camil, J. Petrographie, Chronologie Des Ensembles Granulitiques Archeens Et Formations Associees De La Region De Man (Cote D'ivoire). Implication Pour L'histoire Geologique Du Carton Ouest Africain. Ph.D. Thesis, Univ. Abidjan, Abidjan, Côte d'Ivoire, 1984; 306p.
23. Eglinger, A.; Thébaud, N.; Zeh, A.; Davis, J.; Miller, J.; Parra-Avila, L.A.; Loucks, R.; McCuaig, C.; Belousova, E. New insights into the crustal growth of the Paleoproterozoic margin of the Archean Kenema-Man Domain, West African craton (Guinea): Implications for gold mineral system. *Precambrian Res.* **2017**, *292*, 258–289. [CrossRef]
24. Abouchami, W.; Boher, M.; Michard, A.; Albarède, F. A major 2.1 Ga event of mafic magmatism in West Africa: An early stage of crustal accretion. *J. Geoph. Res.* **1990**, *95*, 17605–17629. [CrossRef]

25. Boher, M.; Abouchami, W.; Michard, A.; Albarède, F.; Arndt, N.T. Crustal growths in West Africa at 2.1 Ga. *J. Geoph. Res.* **1992**, *97*, 345–369. [CrossRef]
26. Taylor, P.N.; Moorbath, S.; Leube, A.; Hirdes, W. Early Proterozoic crustal evolution in the Birimian of Ghana: Constraints from geochronology and isotope geochemistry. *Precambrian Res.* **1992**, *56*, 97–111. [CrossRef]
27. Hirdes, W.; Davis, D.W.; Eisenlohr, B.N. Reassessment of Proterozoic granitoid ages in Ghana on the basis of U/Pb zircon and monazite dating. *Precambrian Res.* **1992**, *56*, 89–96. [CrossRef]
28. Feybesse, J.L.; Milési, J.P.; Verhaeghe, P.; Johan, V. Le domaine de Toulepleu-Ity (Côte d'Ivoire): Une unité birimienne charriée sur les gneiss archéens du domaine de Kenema-Man lors des premiers stades de l'orogène éburnéen. *C. R. Acad. Sci. Paris* **1990**, *310*, 285–291.
29. Milesi, J.P.; Feybesse, J.L. Le gisement d'Ity (Côte d'Ivoire). Calage lithologique et structural. In *Note Technique BRGM-DMM-DEX-UR-93-029*; BRGM: Orléans, France, 1993; 15p.
30. Papon, A. Géologie et minéralisation du Sud-ouest de la Côte d'Ivoire. In *Synthèse des Travaux de L'opération SASCA, 1962–1968*; BRGM-SODEMI: Abidjan, Côte d'Ivoire, 1973; 286p.
31. Monthel, J.; Eulry, M.; Michel, J.C. Le gisement aurifère d'Ity, déjà une longue histoire! *Géochronique* **2002**, *83*, 27–28.
32. Lemoine, S. Evolution Géologique De La Région De Dabakala (NE De La Côte d'Ivoire) Au Proterozoïque Inferieur. Possibilités D'extension Au Reste De La Côte d'Ivoire Et Au Burkina Faso. Unpublished Master's Thesis, University of Clermont-Ferrand, Clermont-Ferrand, France, 1988; p. 388.
33. Ledru, P.; Pons, J.; Milési, J.P.; Feybesse, J.L.; Johan, V. Transcurrent tectonics and polycyclic evolution in the Lower Proterozoic of Sénégal-Mali. *Precambrian Res.* **1991**, *50*, 337–354. [CrossRef]
34. Triboulet, C.; Feybesse, J.L. Les métabasites birimiennes et archéennes de la région de Toulepleu-Ity (Côte d'Ivoire): Des roches portées à 8 kbar (≈24 km) et 14 kbar (≈42 km) au Paléoprotérozoïque. *C. R. Acad. Sci. Paris IIA* **1998**, *327-1*, 61–66.
35. Poty, B.; Leroy, J.; Jachimowicz, L. Un nouvel appareil pour la mesure des températures sous le microscope: L'installation de microthermométrie Chaixmeca. *Bull. Soc. Fr. Mineral. Cristall.* **1976**, *9*, 182–186. [CrossRef]
36. Dubessy, J. Simulation des équilibres chimiques dans le système C-O-H. Conséquences méthodologiques pour les inclusions fluides. *Bull. Min.* **1984**, *107*, 157–168. [CrossRef]
37. Dubessy, J.; Poty, B.; Ramboz, C. Advances in C-H-O-N-S fluid geochemistry based on micro Raman spectroscopic analyses on fluid inclusions. *Eur. J. Miner.* **1989**, *4*, 517–534. [CrossRef]
38. Thiéry, R.; Vidal, J.; Dubessy, J. Phase equilibria modelling applied to fluid inclusions: Liquid-vapour equilibria calculation of the molar volume in the CO_2-CH_4-N_2 system. *Geochim. Cosmochim. Acta* **1994**, *58*, 1073–1082. [CrossRef]
39. Bakker, R.J. Clathrates: Computer programs to calculate fluid inclusions V-X properties using clathrate melting temperature. *Comput. Geosci.* **1997**, *23*, 1–18. [CrossRef]
40. Bowers, T.S.; Helgeson, H.W. Calculation of the thermodynamic and geochemical consequences of non-ideal mixing in the system H_2O-CO_2-NaCl on phase relations in geological systems: Equation of state for H_2O-CO_2-NaCl fluids at high pressures and temperatures. *Geochim. Cosmochim. Acta* **1983**, *47*, 1247–1275. [CrossRef]
41. Bakker, R.J. Adaptation of the Bowers Helgeson (1983) equation of state to the H_2O-CO_2-CH_4-N_2-NaCl system. *Chem. Geol.* **1999**, *154*, 225–236. [CrossRef]
42. Zhang, Y.G.; Frantz, J.D. Determination of the homogenisation temperatures and densities of supercritical fluids in the system NaCl-KCl-$CaCl_2$-H_2O using synthetic fluid inclusions. *Chem. Geol.* **1987**, *64*, 335–350. [CrossRef]
43. Boiron, M.C.; Essarraj, S.; Sellier, E.; Cathelineau, M.; Lespinasse, M.; Poty, B. Identification of fluid inclusions in relation to their host microstructural domains in quartz by cathodoluminescence. *Geochim. Cosmochim. Acta* **1992**, *56*, 175–185. [CrossRef]
44. Mathieu, R. Etude pétrographique, métallographique et lithogéochimique. In *Rapport COGEMA –BUM-DEX-GT-9304*; internal report from a mining company (COGEMA), 2005; 84p.
45. John, T.; Klemd, R.; Hirdes, W.; Loh, G. The metamorphic evolution of the Paleoproterozoic (Birimian) volcanic Ashanti belt (Ghana, West Africa). *Precambrian Res.* **1999**, *98*, 11–30. [CrossRef]
46. Grant, M.A. The Geology of Junction Reef and the Sheahan-Grant Gold Deposit, Mandurama, N.SW. Unpublished B.Sc. (Hons) Thesis, Australian National University, Canberra, Australia, 1988; 121p.
47. Hickey, R.J. The Geology of the Buckhorn Mountain Gold Skarn, Okanogan County, Washington. Unpublished Master's Thesis, Washington State University, Pullman, WA, USA, 1990; 171p.
48. Ettlinger, A.D.; Meinert, L.D.; Ray, G.E. Gold skarn mineralisation and fluid evolution in the Nickel Plate deposit, Hedley district, British Columbia. *Econ. Geol.* **1992**, *87*, 1541–1565. [CrossRef]
49. Brooks, J.W. Petrology and Geochemistry of the McCoy Gold Skarn, Lander County, Nevada. Ph.D. Thesis, Washington State University, Pullman, WA, USA, 1994; 607p.
50. Gunnesch, K.A.; Del Angel, C.T.; Castro, C.C.; Saez, J. The Cu-(Au) skarn and Ag-Pb-Zn vein deposits of La Paz, northeastern Mexico: Mineralogic, Paragenetic, and fluid inclusion characteristics. *Econ. Geol.* **1994**, *89*, 1640–1650. [CrossRef]

51. Myers, G.L. Geology of the Copper Canyon-Fortitude Skarn System, Battle Mountain, Nevada. Ph.D. Thesis, Washington State University, Pullman, WA, USA, 1994; 356p.
52. Wilkie, K.M. Geology and Hydrothermal Evolution of the Beal Mountain Gold Deposit, Silver Bow County, Montana. Ph.D. Dissertation, Washington State University, Pullman, WA, USA, 1996; 371p.
53. Markowski, A.; Vallance, J.; Chiaradia, M.; Fontboté, L. Mineral zoning and gold occurrence in the Fortuna skarn mine, Nambija district, Ecuador. *Miner. Depos.* **2006**, *41*, 301–321. [CrossRef]
54. Kamvong, T.; Zaw, K. The origin and evolution of skarn-forming fluids from the Phu Lon deposit, northern Loei Fold Belt, Thailand: Evidence from fluid inclusion and sulfur isotope studies. *J. Asian Earth Sci.* **2009**, *34*, 624–633. [CrossRef]
55. Block, S.; Ganne, J.; Baratoux, L.; Zeh, A.; Parra-Avila, L.; Jessell, M.; Ailleres, L.; Siebenaller, L. Petrological and geochronological constraints on lower crust exhumation during Paleoproterozoic (Eburnean) orogeny, NW Ghana, West African Craton. *J. Metam. Geol.* **2015**, *33*, 463–494. [CrossRef]
56. Martz, M.; Cathelineau, M.; Mercadier, J.; Boiron, M.-C.; Jaguin, J.; Tarantola, A.; Demacon, M.; Gerbeaud, O.; Quirt, D.; Doney, A.; et al. C-O-H-N fluids circulations and graphite precipitation in reactivated Hudsonian shear zones during basement uplift of the Wollaston-Mudjatik Transition Zone: Example of the Cigar Lake U deposit. *Lithos* **2017**, *294–295*, 222–245. [CrossRef]
57. Coulibaly, Y.; Boiron, M.C.; Cathelineau, M.; Kouamélan, A.N. Fluid immiscibility and gold deposition in the Birimian quartz veins of the Angovia deposit (Yaouré, Ivory Coast). *J. Afr. Earth Sci.* **2008**, *50*, 234–258. [CrossRef]
58. Schwartz, M.O.; Oberthür, T.; Amanor, J.; Gyapong, W.A. Fluid inclusion re-equilibration and P-T-X constraints on fluid evolution in the Ashanti gold deposit, Ghana. *Eur. J. Miner.* **1992**, *4*, 1017–1033. [CrossRef]
59. Yao, Y.; Murphy, P.J.; Robb, L.J. Fluid characteristics of granitoid-hosted gold deposits in the Birimian terrane of Ghana: A fluid inclusions microthermometric and Raman spectroscopic study. *Econ. Geol.* **2001**, *96*, 1611–1643. [CrossRef]
60. Klemd, R.; Hirdes, W.; Olesch, M.; Oberthür, T. Fluid inclusions in quartz pebbles of the gold-bearing Tarkwaian conglomerates of Ghana as guides to their provenance area. *Miner. Depos.* **1993**, *28*, 334–343. [CrossRef]
61. Schmidt Mumm, A.; Oberthür, T.; Vetter, U.; Blenkinsop, T.G. High CO_2 content of fluid inclusions in gold mineralisations in the Ashanti belt, Ghana: A new category of ore forming fluids? A reply. *Miner. Depos.* **1998**, *33*, 320–322. [CrossRef]
62. Wille, S.E.; Klemd, R. Fluid inclusion studies of the Abawso gold prospect, near the Ashanti Belt, Ghana. *Miner. Depos.* **2004**, *39*, 31–45. [CrossRef]
63. Klemd, R.; Hirdes, W. Origin of an unusual fluid composition in Early Proterozoic paleoplacer and lode-gold deposits in Birimian greenstone terranes of West Africa. South African. *J. Geol.* **1997**, *100*, 405–414.
64. Oberthür, T.; Schmidt Mumm, A.; Vetter, U.; Simon, K.; Amanor, J.A. Gold mineralisation in the Ashanti Belt of Ghana; genetic constraints of the stable isotope geochemistry. *Econ. Geol.* **1996**, *91*, 289–301. [CrossRef]
65. Klem, R. Comment on the paper by Schmidt Mumm et al. High CO_2 content of fluid inclusions in gold mineralisations in the Ashanti Belt, Ghana: A new category of ore forming fluids? (Mineralium Deposita 32: 107–118, 1997). *Miner. Depos.* **1998**, *33*, 317–319. [CrossRef]
66. Kazapoe, R.W.; Okunlola, O.; Arhin, E.; Olisa, O. Isotope geochemistry as a tool in the exploration of gold occurrences in Ghana: A review. *Arab. J. Geosci.* **2021**, *14*, 1992. [CrossRef]
67. Ridley, J.R.; Diamond, L.W. Fluid chemistry of lode-gold deposits and implications for genetic models. In *Gold in 2000*; Hagemann, S.G., Brown, P., Eds.; Society of Economic Geologists: Littleton, CO, USA, 2000; Volume 13, pp. 141–162.
68. Hollister, L.S. Enrichment of CO_2 in fluid inclusions in quartz by removal of H_2O during crystal–plastic deformation. *J. Struct. Geol.* **1990**, *12*, 895–901. [CrossRef]
69. Bakker, R.J.; Jansen, J.B.H. Experimental post-entrapment water loss from synthetic CO_2-H_2O inclusions in natural quartz. *Geochim. Cosmochim. Acta* **1991**, *55*, 2215–2230. [CrossRef]
70. Boiron, M.C.; Cathelineau, M.; Banks, D.A.; Fourcade, S.; Vallance, J. Mixing of metamorphic and surficial fluids during the uplift of the Hercynian upper crust: Consequences for gold deposition. *Chem. Geol.* **2003**, *194*, 119–141. [CrossRef]
71. Kerrich, R.; Fyfe, W.S. The gold-carbonate association: Source of CO_2 and CO_2 fixation reactions in Archean lode-gold deposits. *Chem. Geol.* **1981**, *33*, 265–294. [CrossRef]
72. Robert, F.; Kelly, W.C. Ore-forming fluids in Archean gold-bearing quartz veins at the Sigma mine, Abitibi greenstone belt, Quebec, Canada. *Econ. Geol.* **1987**, *82*, 1464–1482. [CrossRef]
73. Groves, D.I. The crustal continuum model for late Archaean lode-gold deposits of the Yilgarn block, Western Australia. *Miner. Depos.* **1993**, *28*, 366–374. [CrossRef]
74. Billa, M. *Calage des Minéralisations Aurifères et Guides de Prospection Pour de Nouveaux Objectifs sur les Permis D'exploration Ity (Côte d'Ivoire)*; Note BRGM: Orléans, France, 1998; Volume 2717, 44p.
75. Phillips, G.N.; Evans, K.A. Role of CO_2 in the formation of gold deposits. *Nature* **2004**, *429*, 860–863. [CrossRef]
76. Mumin, A.H.; Fleet, M.E. Evolution of gold mineralisation in the Ashanti Gold Belt, Ghana: Evidence from carbonate compositions and parageneses. *Miner. Petrol.* **1995**, *55*, 265–280. [CrossRef]

77. Lawrence, D.M.; Treloar, P.J.; Rankin, A.H.; Boyce, A.; Harbidge, P. A fluid inclusion and stable isotope study at the Loulo mining district, Mali, West Africa: Implications for multifluid sources in the generation of orogenic gold deposits. *Econ. Geol.* **2013**, *108*, 229–257. [CrossRef]
78. Kazapoe, R.W.; Okunlola, O.; Arhin, E.; Olisa, O.; Harris, C.; Kwayisi, D.; Torkorno, S.; Amuah, E.E.Y. Geology and isotope systematics of gold deposits in the Abansuoso area of the Sefwi belt, southwestern Ghana. *Geol. Ecol. Landsc.* **2022**, *8*, 423–444.
79. Lüders, V.; Klemd, R.; Oberthür, T.; Plessen, B. Different carbon reservoirs of auriferous fluids in African Archean and Proterozoic gold deposits: Constraints from stable carbon isotopic compositions of quartz-hosted CO_2-rich fluid inclusions. *Miner. Dep.* **2015**, *50*, 449–454. [CrossRef]
80. Li, H.; Wang, Q.; Yang, L.; Weng, W.; Deng, J. Disseminated gold mineralisation under varied redox conditions: Constraints from microscopic observation, geochemistry, and thermodynamic modeling on fluid-rock interactions in lamprophyres, Zhenyuan gold deposit. *Chem. Geol.* **2023**, *635*, 121627. [CrossRef]
81. Kokh, M.; Akinfiev, N.; Pokrovski, G.; Salvi, S.; Guillaume, D. The role of carbon dioxide in the transport and fractionation of metals by geological fluids. *Geochim. Cosmochim. Acta* **2017**, *197*, 433–466. [CrossRef]
82. Petrella, L.; Thébaud, N.; Evans, K.; Lamme, C.; Ochiinti, S. The role of competitive fluid-rock interaction processes in the formation of high-grade gold deposits. *Geochim. Cosmochim. Acta* **2021**, *313*, 38–54. [CrossRef]
83. Zhou, H.; Sun, X.; Cook, N.J.; Lin, H.; Fu, J.; Zhong, R.; Brugger, J. Nano-to-micron-scale particulate gold hosted by magnetite: A product of gold scavenging by bismuth melts. *Econ. Geol.* **2017**, *112*, 993–1010. [CrossRef]
84. Ma, T.; Chen, C.; Zhang, Y.; Yang, Y.; Liu, X.; Lai, X.; Gu, Y. Mineralogy and mineral chemistry of Bi–Te minerals: Constraints on mineralisation process of the Dulanggou gold deposit, Dadu River Metallogenic Belt, China. *Ore Geol. Rev.* **2024**, *169*, 106091. [CrossRef]
85. Einaudi, M.T.; Meinert, L.D.; Newberry, R.J. *Skarn Deposits*; Economic Geology Publishing Company: Littleton, CO, USA, 1981; Volume 75, pp. 317–391.
86. Meinert, L.D.; Dipple, G.M.; Nicolescu, S. *World Skarn Deposits*; Society of Economic Geologists: Littleton, CO, USA, 2005; Volume 100, pp. 299–336.
87. Sheppard, S.; Walshe, J.L.; Poolet, G.D. Noncarbonate, skarnlike, Au-Bi-Te mineralisation, Lucky Draw, New South Wales, Australia. *Econ. Geol.* **1995**, *90*, 1553–1569. [CrossRef]
88. Nörteman, M.F.J.; Mücke, A.; Weber, K.; Meinert, L.D. Mineralogy of the Navachab deposit, Namibia: An unusual Au-bearing skarn in high grade metamorphic rocks. *Commun. Geol. Surv. Namib.* **2001**, *12*, 149–156.
89. Bosse, H.R.; Gwosdz, W.; Lorenz, W.; Markwich, H.; Roth, W.; Wolff, F. Limestone and dolomite resources of Africa. *Geol. Jahrb.* **1996**, *D102*, 3–532.
90. Bering, D.; Brinckmann, J.; Camara, N.; Diawara, M.; Gast, L.; Keita, S. *Evaluation de L'inventaire des Ressources Minérales de Guinée*; Bundesanstalt für Geowissenschaften und Rohstoffe: Hannover, Germany, 1998; 109p.
91. Schwartz, M.O.; Melcher, F. The Falémé Iron District, Senegal. *Econ. Geol.* **2004**, *99*, 917–939. [CrossRef]
92. *IAMGOLD Sadiola Gold Mine, Mali: Geology and Mineralisation*; Report; IAMGOLD Corp.: Toronto, ON, Canada, 2008.
93. Konate, S.I.M.; Bolarinwa, A.T.; Kazapoe, R.W.; Bouare, M.L.; Traore, E.M.; Ngiamte, G.L.; Kouagou N'Dah, N.D. A review of the current state of knowledge on gold mineralization in Mali, Western Africa. *Geol. Ecol. Landsc.* **2024**, 1–25. [CrossRef]
94. Béziat, D.; Dubois, M.; Débat, P.; Nikiéma, S.; Salvi, S.; Tollon, F. Gold metallogeny in the Birimian craton of Burkina Faso (West Africa). *J. Afr. Earth Sci.* **2007**, *50*, 215–233. [CrossRef]
95. Oberthür, T.; Vetter, U.; Schmidt Mumm, A.; Weiser, T.; Amanor, J.A.; Gyapong, W.A.; Kumi, R.; Blenkinsop, T.G. The Ashanti gold mine at Obuassi, Ghana: Mineralogical, geochemical, stable isotope and fluid inclusion studies and the metallogenesis of the deposit. *Geol. Jahrb.* **1994**, *100*, 31–129.
96. Klemd, R.; Oberthür, T.; Ouedraogo, A. Gold-telluride mineralisation in the Birimian at Diabatou, Burkina Faso: The role of CO_2-N_2 fluids. *J. Afr. Earth Sci.* **1997**, *24*, 227–239. [CrossRef]
97. Groves, D.I.; Phillips, G.N. The genesis and tectonic control on Archaean gold deposits of the western Australian shields—A metamorphic replacement model. *Ore Geol. Rev.* **1987**, *2*, 287–322. [CrossRef]
98. Naden, J.; Shepherd, T.J. Role of methane and carbon dioxide in gold deposition. *Nature* **1989**, *342*, 793–795. [CrossRef]
99. Groves, D.I.; Barnicoat, A.C.; Barley, M.; Cassidy, K.F.; Fare, R.J.; Hagemann, S.G.; Ho, S.E.; Hronsky, J.M.A.; Mikucki, E.J.; Mueller, A.G. *Sub-Greenschist-to Granulite-Hosted Archaean Lode-Gold Deposits of the Yilgarn Craton: A Depositional Continuum from Deep-Sourced Hydrothermal Fluids in Crustal-Scale Plumbing Systems*; Publication of the University of Western Australia: Crawley, Australia, 1992; Volume 22, pp. 325–337.
100. Goldfarb, R.J.; Leach, D.L.; Rose, S.C.; Landis, G.P. Fluid inclusion geochemistry of gold-bearing quartz veins of the Juneau gold belt, southeastern Alaska: Implications for ore genesis. In *The Geology of Gold Deposits: The Perspective in 1988*; Keays, R., Ramsay, R., Graves, D., Eds.; Society of Economic Geologists: El Paso, TX, USA, 1989; Volume 6, pp. 363–375.
101. Goldfarb, R.J.; Snee, L.W.; Pickthorn, W.J. Orogenesis, high-T thermal events, and gold vein formation within metamorphic rocks of the Alaskan Cordillera. *Miner. Mag.* **1993**, *57*, 363–375. [CrossRef]

102. Van Reenen, D.D.; Pretorius, A.I.; Roering, C. Characterization of fluids associated with gold mineralisation and with regional high-grade retrogression in the Limpopo belt. *Geochim. Cosmochim. Acta* **1994**, *58*, 1147–1159. [CrossRef]
103. Santosh, M.; Nadeau, M.; Javoy, M. Stable isotopic evidence for the involvement of mantle-derived fluids in Wynad gold mineralisation. *J. Geol.* **1995**, *103*, 718–728. [CrossRef]
104. Klein, E.L.; Fuzikawa, F.; Koppe, J.C. Fluid inclusion studies on Caxias and Areal gold mineralisations, Sao Luis Craton, Northern Brazil. *J. Geochem. Explor.* **2000**, *71*, 51–72. [CrossRef]